DEGREE PROJECT

FE-Modelling of Composite Girder tests

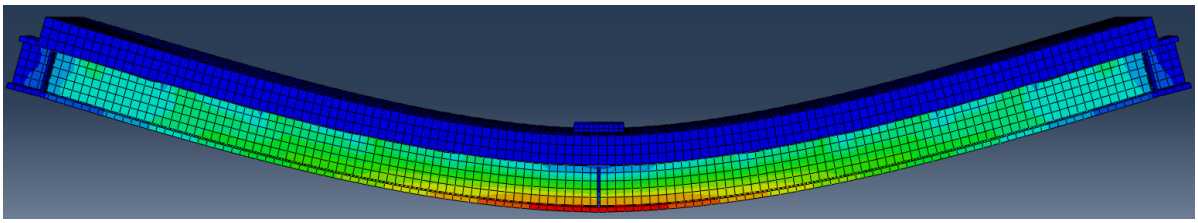

Ola Bergstedt
Holger Berggren

Civil Engineering, master's level
2024

Luleå University of Technology
Department of Civil, Environmental and Natural Resources Engineering

LULEÅ UNIVERSITY OF TECHNOLOGY

[This page intentionally left blank]

Preface

"*You may delay, but time will not.*"
- Benjamin Franklin, US statesman, author, and scientist

We would like to express our gratitude to our examiner, Prof. Peter Collin, for providing us with the opportunity to work with this project. We also want to thank our supervisor, PhD student Victor Vestman, for the time he has dedicated to guiding us through this project. Additionally, our thanks go to Adj. Prof. Robert Hällmark for assisting us in compiling data from the laboratory tests.

Ola Bergstedt
Skellefteå, January 2024

Holger Berggren
Lomma, January 2024

Abstract

Many of the existing steel-concrete bridges may need to be strengthened, as heavier vehicles are allowed on the Swedish roads. These bridges could possibly be strengthened by post-installing shear connectors. The shear connectors may enhance the load-bearing capacity through a higher degree of composite action between the steel and concrete interface.

For post-installing of shear connectors, it is advantageous to use a method that allows for installation from underneath the bridge as it avoids disrupting the traffic flow. The authors have hence focused on a shear connector called coiled spring pin (CSP); a sheet of metal rolled into a coil. It's inserted by hydraulic jacking into a pre-drilled hole and maintained in position due to radial spring force, avoiding the need for welding.

Information and data are collected from beam tests performed at Luleå technical university, the Eurocodes and literature.

This study investigates and identifies the behaviour and characteristics of a partial composite girder reinforced with CSPs. The study compares the results obtained from the laboratory tests and the FEM-simulations. Furthermore, this research examines the factors that contribute to the accuracy of the FEM models and investigates the influence of the CSP placement on the overall load-bearing capacity.

Both the FEM simulations and laboratory tests indicate that the girders exhibit strength benefits from applying CSPs. An optimal position for the connectors could not be determined, as the results presented in the simulations was not proved by the laboratory tests. The simulations indicate benefits with central placed CSPs, in contrast to the laboratory test where no differences from the placement were shown, although only two test setups were used.

Keywords: Shear connector; Post-installed; Coiled spring pins; Composite girder; Partial composite action; Finite element method.

Sammanfattning

Många av de befintliga stål-betongbroarna behöver förstärkas eftersom tyngre fordon tillåts på de svenska vägarna. Förstärkning av dessa broar kan uppnås genom efterinstallation av tvärkraftsförbindare. Dessa förbättrar avsevärt bärförmåga genom en hög grad av samverkan mellan stål- och betongytorna.

För efterinstallation av tvärkraftsförbindare är det fördelaktigt att använda en metod som möjliggör installationen från undersidan av bron eftersom det undviker störningar av trafiken. Författarna har fokuserat på tvärkraftsförbindare som kallas coiled spring pin (CSP), en plåt rullad till en spole. De installeras med en hydrualisk domkraft i ett förborrat hål och hålls på plats med radial fjäderkraft, vilket undviker behovet av svetsning.

Information och data samlas från ett balktest utfört på Luleå tekniska universitet, Eurokoder och litteratur.

Denna avhandling undersöker och identifierar beteendet och egenskaperna hos en partiell samverkansbalk förstärkt med CSP. Studien jämför resultaten från laboratorietesterna med FEM-simuleringarna. Dessutom undersöks de faktorer som bidrar till noggrannheten hos FEM-modellerna samt hur bärförmågan påverkas utifrån tvärkraftsförbindarnas placering.

Både FEM-simuleringarna och laboratorietesterna visar fördelar i bärförmåga efter att tvärkratsförbindare applicerats. Den optimala positioneringen kunde inte fastställas eftersom resultaten från simuleringarna inte bevisades av laboratorietesterna. Simuleringarna indikerar fördelar med centralt placerade tvärkraftsförbindare, i motsats till laboratorietestet där inga skillnader kunde erhållas från placeringen.

Notations

Roman upper letters

Symbol	Description
A	Area
E	Modulus of elasticity
E_{cm}	Secant modulus of elasticity of concrete
F	Force
I	Moment of inertia
I_{NC}	Moment of inertia, non-composite action
I_{FC}	Moment of inertia, full composite action
K	Coefficient for stress in steel
L	Length
M	Bending moment
U	Displacement

Roman lower letters

Symbol	Description
d_c	Concrete damage parameter, compression
d_t	Concrete damage parameter, tension
e	Distance to centre of gravity
f_{b0}	Initial equibiaxial compressive yield stress
f_{c0}	Initial uniaxial compressive yield stress
f_{cm}	Mean value of concrete cylinder compressive strength
f_u	Ultimate tensile stress
f_y	Yield stress
h	height
k	Coefficient for compressive stress in concrete
w	Width

Greek letters

Symbol	Description
ε	Strain
ε_c	Compressive strain in the concrete
ε_{c1}	Compressive strain in the concrete at peak stress
$\varepsilon_{c,in}$	Inelastic tensile strain
$\varepsilon_{c,pl}$	Plastic tensile strain
ε_{sh}	Strain hardening value
ε_t	Tensile strain in the concrete
$\varepsilon_{t,ck}$	Cracking strain
ε_u	Ultimate tensile strain
η	Ratio
μ	Friction coefficient
ν	Poisson's ratio
σ	Stress
σ_c	Compressive stress
σ_{cu}	Compressive stress in the concrete at ultimate compressive strain
$\sigma_{b.l.f}$	Stress, bottom of lower flange
$\sigma_{b.u.f}$	Stress, bottom of upper flange
$\sigma_{l.f}$	Stress, lower flange
σ_t	Tensile stress
$\sigma_{t.c}$	Stress, top concrete
$\sigma_{t.l.f}$	Stress, top of lower flange
$\sigma_{t.u.f}$	Stress, top of upper flange
$\sigma_{u.f}$	Stress, upper flange
σ_w	Stress, web
Φ	Reinforcement diameter

Abbreviations

Abbreviation	Description
cc	Centre-to-centre
CDP	Concrete damage plasticity
CS	Cross-section
CSP	Coil spring pin
FC	Full composite
FEM	Finite element method
G1	Girder 1
G2	Girder 2
G3	Girder 3
NC	Non-composite
PC	Partial composite

Table of contents

1 Introduction

1.1 Background

Today, the bridges are exposed to greater loads as heavier vehicles are allowed on the Swedish roads. At the same time, the amount of traffic also increases (Olsson, 2017). This means that the bridges in Sweden will be loaded more heavily and with greater frequency. The existing bridges may have problems coping with these new loads, as they are designed by older regulations and conditions.

For the bridges that do not fulfil the new requirements there are two alternatives, replace the bridge or strengthen it. Building new bridges is considered a solution that should be avoided as it is both expensive and most likely has a large environmental impact. However, strengthening existing bridges is considered a solution that can be both environmentally friendly and cost-effective (Hällmark, et al., n.d).

One solution to strengthening the existing bridges is by using post-installed shear connectors. The shear connectors are placed through the top flange and into the concrete deck and can increase the total load capacity due to composite action (Hällmark, 2018).

A possible cost-effective substitute for full composite action is partial composite action. Partial composite action still achieves an increase of bending stiffness of the cross-section, but with a significantly reduced amount of shear connectors (Kwon, 2008). In the Eurocode SS-EN 1994-1-1 (2005) there are generally standards for partial composite action, which can be a time and cost-effective solution for components that do not need full capacity increase. However, in the bridge industry there are only standardised methods for full composite action. The existing standards for the other disciplines cannot be directly implemented on bridges, due to different dimensions and a more critical fatigue load (Hällmark, et al., n.d). The research presented in this project is intended to contribute to knowledge and future design rules for partial composite action in the bridge industry.

1.2 Objectives

This thesis is intended to support a research project aiming at establishing reliable design guidelines for partial composite action, for existing bridges. The primary objective of the report is to identify the behaviour and characteristics of girders, both with and without shear connectors.

1.2.1 Research questions

A) What is the behaviour of a girder strengthened with coiled spring pins in terms of stress, displacement, and slip?
B) How does the placement of CSPs impact the total strengthening?
C) Do the results from the simulated girder in Abaqus correspond to the test results from the laboratory tests?
D) Which factors impacts the accuracy of FEM simulations for this type of test setup?

1.3 Limitations and delimitations

- In this report, only shear connectors of the type coiled spring pins are evaluated. There is a lot of existing research on other types of connectors, but this is only briefly mentioned in this report.
- The models in this thesis are solely applicable to road traffic bridges, and not to railway bridges. This is because the Eurocode SS-EN 1993-2 (2017) stipulates that for railway bridges and structures subjected to seismic loads, friction should not be considered.
- The thesis is limited to one span, simply supported beams.
- The thesis mainly focuses on load levels within the elastic region, specifically for the load 350 kN.
- When subjected to a load, the beam undergoes both horizontal and vertical displacement, known as slip and uplift. This thesis, however, only addresses slip.

1.4 Earlier research

For parts of the content in this thesis, there is plenty of previous research. Composite action in general is well documented and there are rules for both full composite action and partial composite action in SS-EN 1994-1-1 (2005). However, for bridges the Eurocodes only cover full composite action and regulations for partial composite action are excluded.

Extensive research has been conducted to evaluate the effects of post-installed shear connectors to achieve partial composite action. For instance, a research team at the University of Texas has done numerous comprehensive studies and tests to verify the results from various types of shear connectors (Kwon, 2008).

Most of the research on coiled spring pins (CSPs) has been conducted at Luleå University of Technology, by Doctor Hällmark, Professor Collin and Doctoral Student Vestman. Master theses on CSPs have also been composed at the university; Olsson (2017), Stahlin (2019) and Tjernberg (2022) have all carried out research on the subject.

1.5 Method

The execution has been preliminarily divided into six major sub-moments:

A literature study, compiling a wide range of existing research.

(1) Report writing.
(2) A learning period of the software Abaqus FEM before the real test models could be composed.
(3) Modelling and simulating of the girders in Abaqus.
(4) Analytical hand calculations to verify the results from the FEM models.
(5) Results and analysis with a comparison between the different methods to evaluate the differences and determine factors of big influence.

Both authors have actively contributed to all aspects of this project, including the research, calculations, modelling, simulations, and written content, so that the workload is divided equally. This has been ensured by maintaining frequent communication and mutual involvement in all project components.

1.6 Structure of thesis

Chapter 1, Introduction - Introduces the subject with background and previous research. The execution of the project is described, and the main objectives are presented.

Chapter 2, Theory - Explains what composite action is and its application in bridge construction.

Chapter 3, Test of composite girders with coiled spring pins - Presents the outcome of the preceding laboratory tests conducted on two girders, one with non-composite action and one with partial composite action.

Chapter 4, Finite element method of on composite girders - Describes the methodology employed for the FEM simulations in Abaqus and detailing the chosen input.

Chapter 5, Hand calculations - Presents a concept of simple and approximated hand calculations for the different girders. The calculations focus on displacement and stress.

Chapter 6, Factors that may impact the accuracy of the FEM simulations - Introduces three factors that may affect the accuracy of the FEM simulations.

Chapter 7, Laboratory tests - Presents the results from the previously conducted laboratory tests.

Chapter 8, Results - Compilation of the results from the preceding laboratory tests, hand calculations and FEM simulations.

Chapter 9, Analysis and discussion - Discussion and analysis about the results presented in chapter 8.

Chapter 10, Conclusions and recommendations - Conclusions connected to the objectives presented in chapter 1 and recommendations on further research.

2 Theory

2.1 Composite action

Composite action in structures refers to the combination of multiple elements within a cross section, enhancing the overall flexural rigidity farther than the sum of the individual elements' rigidity. The cross-sectional elements can be composed of either the same or varying materials, but when referring to composite bridges the members usually consist of concrete and steel. Making use of composite action is an efficient way of utilising the compressive strength of the concrete and the tensile strength of the steel (Vestman, 2023).

For the non-composite versions, the strain emerges for both compressive and tension forces for each material, this is in contrast with full composite action where the concrete is only subjected to strain from compressive forces, see Figure 2.1.

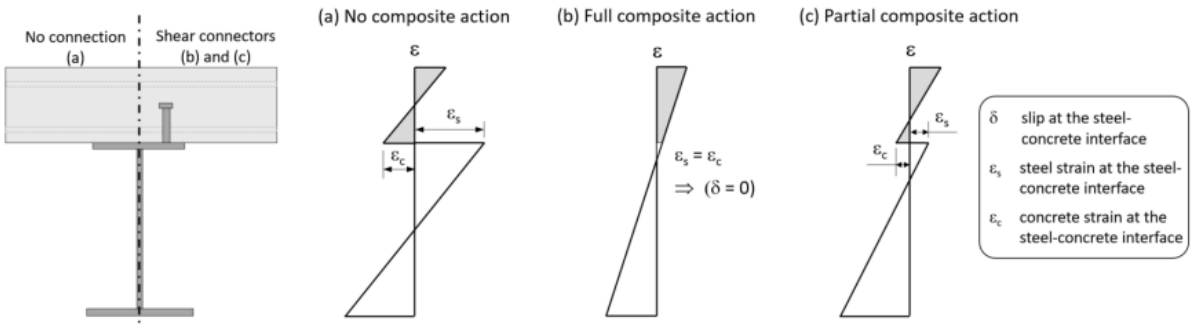

Figure 2.1: Illustration of strain a) without composite action, b) full composite action, c) partial composite action (Hällmark et al., n.d.)

2.1.1 Non-composite action

The theory behind non-composite action is that the concrete and steel act as individual members, and thus only inherit the individual flexural rigidity of said elements. In practice there is always partial composite action between the members because of frictional forces acting between the layers (Norlin, n.d.). The friction and other interlocking factors are however neglected when designing, in accordance with SS-EN 1994-2 (Vestman, 2023).

2.1.2 Full composite action

Full composite action between a steel girder and a concrete slab can be accomplished by ensuring that an adequate number of shear connectors are installed. This will reduce the slip to near zero, making the structure behave as one component and increase the efficiency in load transfer. Slip can be described as the displacement at the interface between the members (Kwon, 2008).

A comparison of a steel-concrete girder with and without composite action is illustrated in Figure 2.2 below.

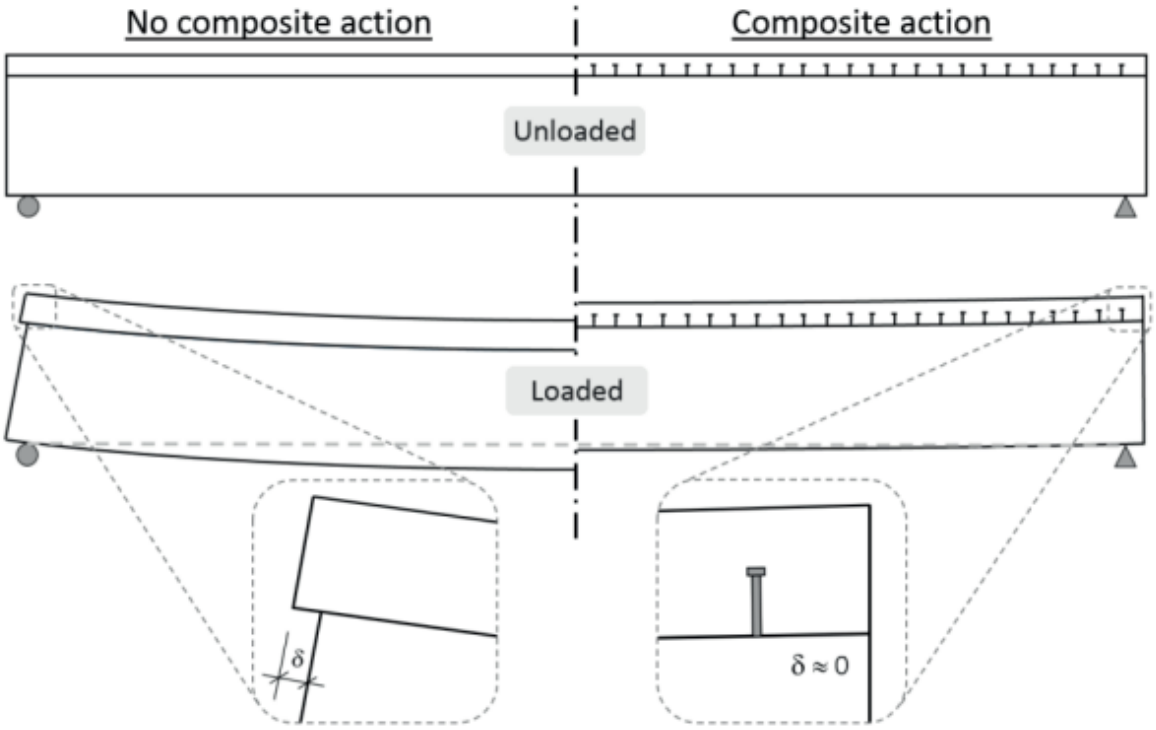

Figure 2.2: Non-composite action versus composite action (Hällmark, 2018)

2.1.3 Partial composite action

As the name suggests, partial composite action falls between the two extremes of non-composite action and full composite action. This implies that while the specimens interact with each other, they do not fully achieve the extent of full composite action.

The research in this thesis is limited to cross sections with partial composite action, as the focus is on post-installation of shear connectors, aiming to strengthen existing bridges.

According to Kwon (2008), partial composite action has been demonstrated as a cost-effective substitute for full composite action. The total amount of shear connectors can be reduced by approximately 50 to 70 percent of the shear connectors commonly required for full composite action, while still increasing the load-carrying capacity by up to 50 percent.

2.1.4 Theoretical explanation of composite action

The stiffness of a whole cross-section can be increased if composite action is used (Vestman, 2023). This can be shown by comparing the moment of inertia for two cases.

For a rectangular cross section, the moment of inertia is calculated as (Isaksson & Mårtensson, 2019):

$$I = \Sigma \frac{wh_i^3}{12} \qquad (2.1)$$

In Figure 2.3, the same structure is shown but the only difference is that case (b) is assumed to have full composite action between each section in contrast to case (b). This will affect the calculation of the moment of inertia for the two cases. Case (a) is handled as the sum of five components and case (b) as one whole structure.

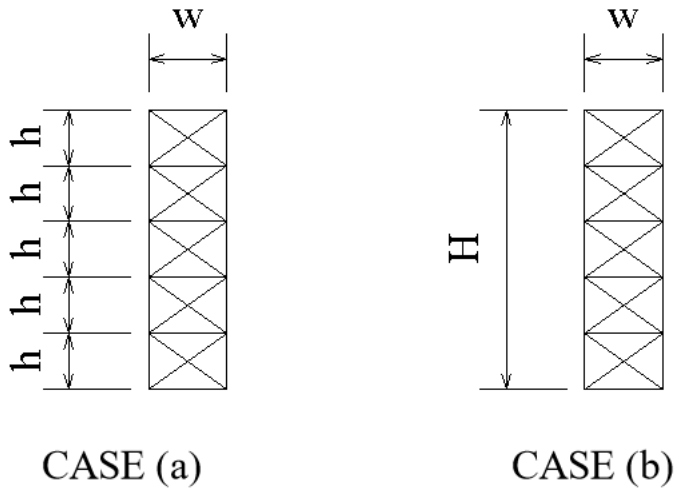

Figure 2.3: Illustration of two structures with different composite action. Based on (Vestman, 2023)

For the case presented in Figure 2.3, the moment of inertia is calculated with the equations below.

Moment of inertia case (a), non-composite action:

$$I_{NC} = \Sigma \frac{wh_i^3}{12} = 5\frac{wh^3}{12} \quad (2.2)$$

Moment of inertia case (b), full composite action:

$$I_{FC} = \frac{wH^3}{12} = \frac{w(5 \cdot h)^3}{12} = 125\frac{wh^3}{12} \quad (2.3)$$

The ratio between the two cases:

$$\frac{I_{FC}}{I_{NC}} = 25 \quad (2.4)$$

Equation 2.4 shows how much the degree of composite action can affect the moment of inertia. However, this calculation only covers one specific case, with five elements and a rectangular cross section. In general, the beam with composite action always achieves a higher moment of inertia, thus:

$$H^3 > \Sigma h_i^3 \quad (2.5)$$

2.2 Composite bridges

Composite bridges have been built since the 1970s and are today a widely used construction method for bridges (Collin et al., 2012). The bridge type contains a concrete deck, steel girders and shear connectors that connects the two materials, see Figure 2.4. The principle of the construction method is utilising the concrete for compressive forces and the steel for tensile forces. By combining and using the different material attributes, a much higher bending resistance is obtained (El Sarraf et al., 2013).

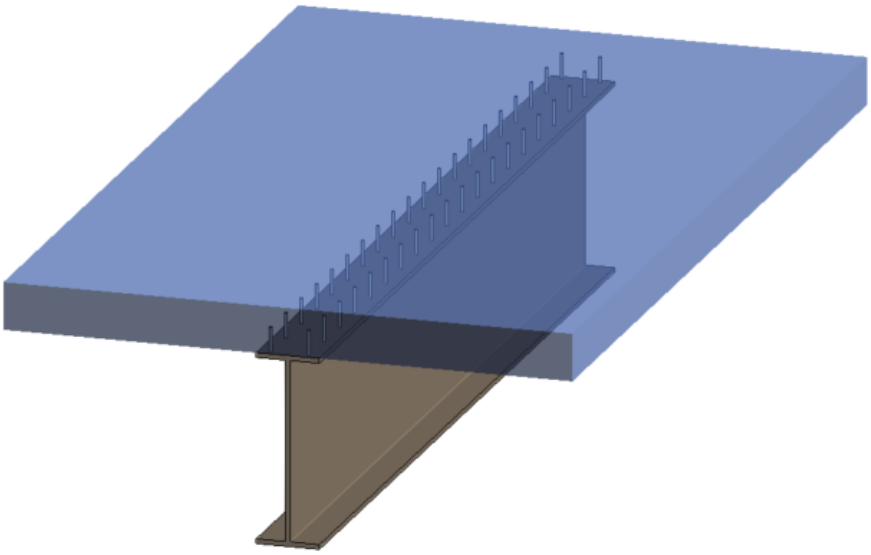

Figure 2.4: Concept of a composite bridge

2.3 Shear connectors

To achieve composite action, high demands are placed on the shear connectors. They should have enough strength, stiffness, and ductility to be able to resist all forces that appears between the concrete and the steel (Vestman, 2023). There are several different types of shear connectors that can be used to achieve composite action, see Figure 2.5. For new bridges it is most common to place welded headed shear studs (a) on top of the steel flange before the concrete casting is done. However, for post installing of shear connectors this solution has some disadvantages. To install the welded headed shear studs, appropriately sized holes need to be drilled to allow access for welding. Given that the installation occurs on top of the bridge, specifically on the road, certain sections or even the entire bridge may need to be closed during construction (Hällmark, 2018).

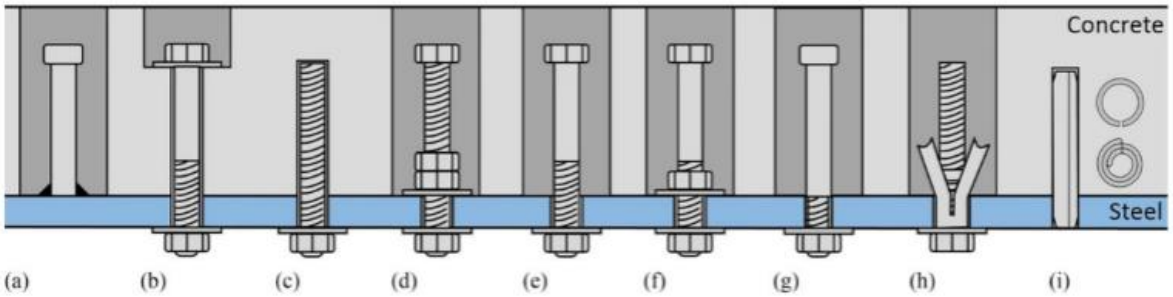

Figure 2.5: Examples of post-installed shear connectors (Hällmark et al., n.d)

To strengthen existing bridges, it can be beneficial to choose shear connectors that can be installed from below the bridge with a low impact on the driving traffic. Research has been done to evaluate different options, for instance, Kwon (2008) did tests on adhesive anchors that could be a valid option. However, for this thesis, only the connector of the type coiled spring pin is evaluated.

The coiled spring pins that have been used in bridge projects so far are steel plates of 2,2 mm that are rolled up to reach a diameter of 20 mm, see Figure 2.6. The installation is performed by pushing up connectors with a hydraulic jack through pre-drilled holes. The connectors stay in place due to the radial spring force in the CSPs and no other fasteners are required (Hällmark, 2018).

Figure 2.6: Illustration of a coiled spring pin (Spirol, 2022)

3 Test of composite girders with coiled spring pins

At Luleå University of Technology, laboratory tests were performed in 2018 to evaluate the behaviour of coiled spring pins as shear connectors.

The tests were conducted on two girder specimens. Initially, they were loaded as non-composite girders, reaching load levels slightly below the yield strength of the steel. The purpose of this was to study the elastic behaviour of a corresponding non-composite girder, and to create a slip between the steel and concrete (Hällmark et al., 2021).

Following this, CSPs were installed to strengthen the girders, and two additional tests were conducted. The first test matched the previous load level, and the girders were then supposed to be loaded to failure but failed to do so because of limitations in the test setup (Hällmark et al., 2021).

3.1 Test setup

The test setup involves a simply supported girder subjected to three-point bending, as illustrated in Figure 3.1. Three-point bending was selected over four-point bending to avoid potential non-conservative frictional shear connections or other interlocking forces. Measurements were taken at the support locations (A, B), the quarter points (QA, QB), and the midspan (MB) as presented in Figure 3.1. In order to analyse the bending stiffness of the specimen, two wire gauges were positioned at the midspan (MB) to measure the vertical displacement (Hällmark et al., 2021).

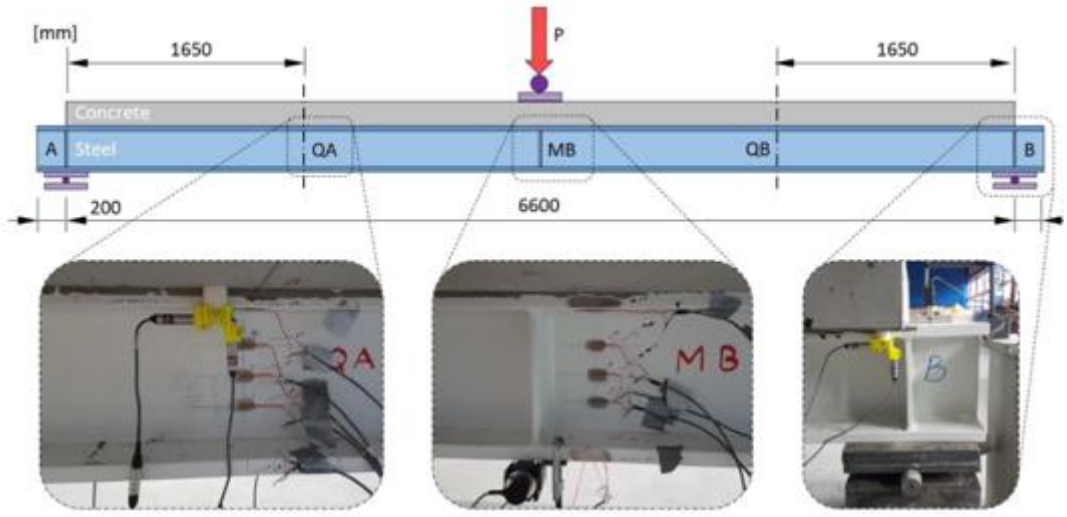

Figure 3.1: Test set-up (Hällmark et.al., 2021)

3.2 Dimensions

The dimensions of the steel girder and the concrete deck are illustrated in Figure 3.2 and Figure 3.3. The figures are drawn according to information in Hällmark et al., (2021).

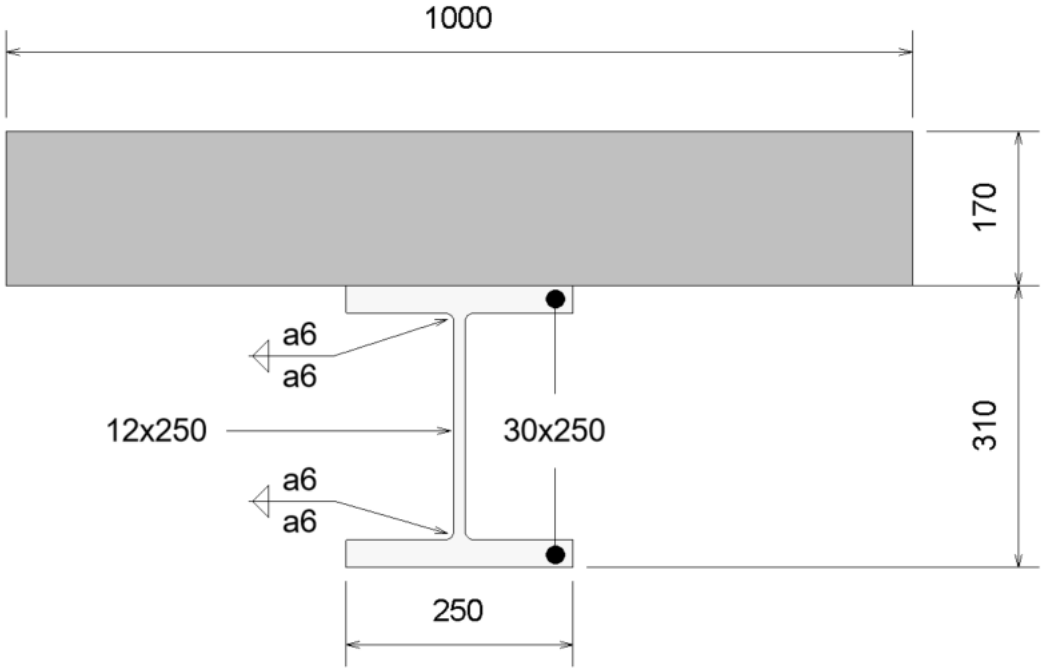

Figure 3.2: Dimensions of the steel girder and the concrete deck

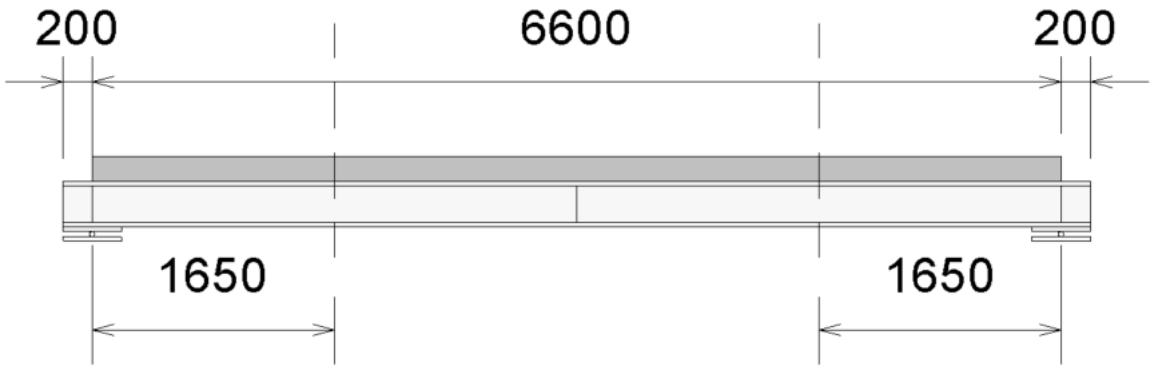

Figure 3.3: Length of steel girder and concrete deck

3.3 Material properties

The material properties of the steel and concrete are presented in Table 3.1 and Table 3.2 below, based on Hällmark et al., (2021).

3.3.1 Steel

Table 3.1: Steel properties

Part	Grade	R_{eh} [MPa]	R_m [MPa]	Elongation [%]
Web	S355K2C+N	447	579	29
Flanges	S355J2	407	541	27
Stiffeners	S355J2	407	541	27
Rebars	B500B	500	-	-
CSP	AISI 6150	1516	1606	5

3.3.2 Concrete

Table 3.2: Concrete properties

C35/45	Girder 1 [MPa]	Girder 2 [MPa]
f_{ccm}	54,8	51,5
$f_{ctm,sp}$	4,4	4,3
E_{cm}	34300	33600

3.4 Placement of coiled spring pins

The placement of the coiled spring pins differs between Girder 1 and Girder 2. On the first beam, connectors are evenly distributed in six pairs on each side, as illustrated in Figure 3.4. For Girder 2, the CSPs are placed in a zigzag pattern where the first eight connectors have a cc distance of 180 mm, and the last four have a cc distance of 360 mm, see Figure 3.5. The distance between the rows of CSPs is 150 mm and the first connector is placed in the middle between the first stirrups (Hällmark et al., 2021), see Appendix A for stirrup placement.

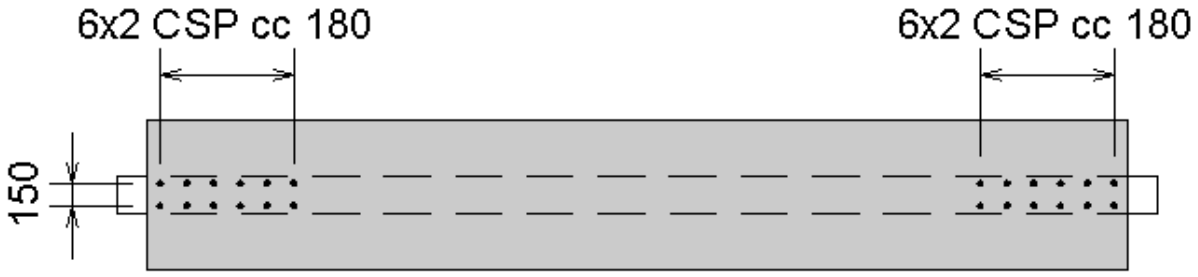

Figure 3.4: Placement off coiled spring pins on Girder 1

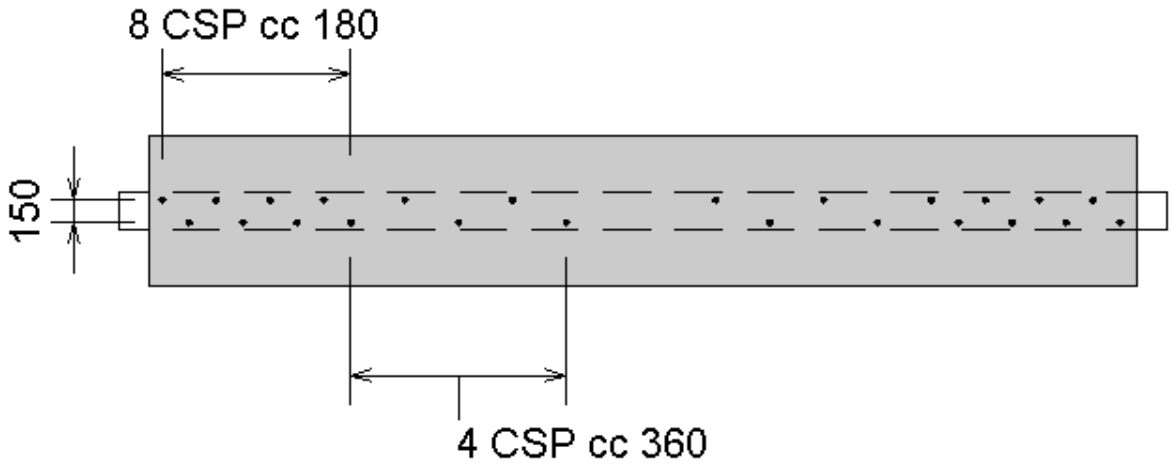

Figure 3.5: Placement of coiled spring pins on Girder 2

3.5 Load in test setup

In the laboratory, five different phases were used for applying the load. The phases from number 1 to 3b were conducted on the girders without the use of coiled spring pins, while phases 4 and 5 were conducted on CSP strengthened girders. Between each phase, the load was removed to be able to restart each phase with no applied force, see Table 3.3 for exact values (Hällmark et al., 2021). For phase 5 the intention was to load the girders until failure, but the test was limited by the midspan deformations distance down to the floor, thus no ultimate failure data is available. In this thesis the primary focus is on phase 4 where the beam is subjected to a load of 350 kN. The secondary focus is on phase 3a and 5, the first is used to replicate the behaviour of full composite action, and the latter is supposed to be the beam loaded to failure.

Table 3.3: Load in test setup

Phase number	G1 Force [kN]	G2 Force [kN]
1	0 – 220	0 - 220
2	0 – 250	0 - 250
3a	0 – 350	0 - 350
3b	-	0 - 420
4	0 – 350	0 - 350
5	0 – 870	0 - 870

4 Finite element method on composite girders

A FEM model was created in Abaqus with the intention of simulating the beam tests presented in chapter 3.

4.1 Dimensions

The FEM model dimensions are based on the laboratory test presented in chapter 3. The steel girder and the concrete deck are modelled according to Figure 3.2 and Figure 3.3, an illustration of the geometry is presented in Figure 4.1. Information about the reinforcement in the concrete deck and the stiffeners on the steel girder is found in Appendix A.

To reduce the execution time for the FEM model, two simplifications were made regarding the reinforcement. For the transverse reinforcement, n-stirrups were chosen instead of using double b-rebars, see Appendix D. The anchoring length angle for the rebars is also simplified. In the created model, the anchoring length is placed with right angles, this differs from the original drawings.

In the laboratory test two welded headed studs was added to attach the concrete cast to the steel beam, however for the FEM simulation this was simplified as the studs are neglected.

The supports are not created as separate parts in Abaqus, instead they are defined as a boundary condition that are placed along the intended contact line. When a support is created as a part, the calculations must be recalculated every time there is a displacement of the beam, thus the contact node on the beam moves away from the contact surface of the support (Vestman, V. Personal communication, 27 November 2023). The simplification of creating the supports in the form of a linear boundary condition proved to result in faster run time with fewer errors. Hower in practice, it is expected to be displacements between the beam and the support, but these are assumed to have a small impact on the total results and are therefore neglected in this phase.

The coiled spring pins are modelled as springs between two surfaces. This is implemented by using the coupling constraints in Abaqus, that connects a reference node with a group of nodes (Dassault Systèmes, 2014). The reference nodes are placed in the lower edge of the upper flange with a corresponding point in the lower edge of the concrete deck. The reference nodes in the steel and the concrete are then connected with the stiffness presented in chapter 4.2.3, this connection is intended to represent the behaviour of a coiled spring pin.

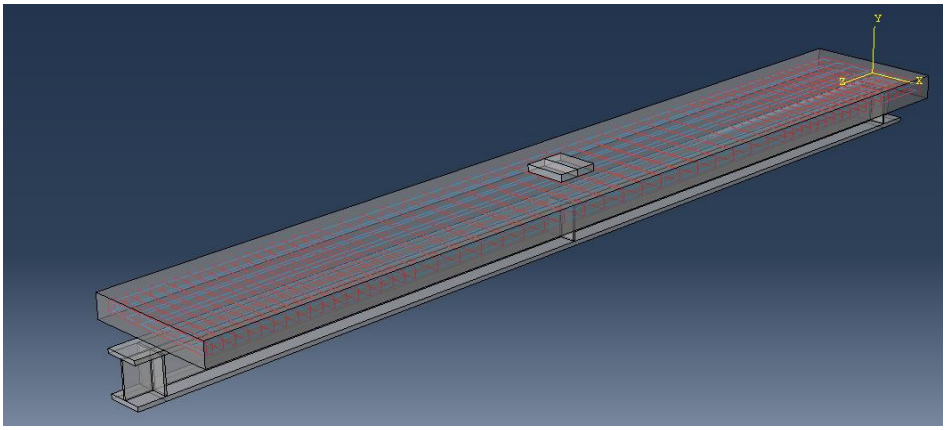

Figure 4.1: FEM model in Abaqus of the girder

4.2 Material properties

In the context of finite element analysis, properly defining material properties is essential to accurately simulate the behaviour of a structure, therefore complete elastic and plastic properties are defined for all materials.

4.2.1 Steel

To define the steel material, the input of mechanical properties, such as the elastic and plastic behaviour must be provided. For the elastic behaviour, input of the modulus of elasticity and Poisson's ratio is required. According to SS-EN 1993-1-1, the modulus of elasticity is consistent for all steel grades in structural design. Poisson's ratio is also determined in accordance with SS-EN 1993-1-1, see Table 4.1.

To present the material's deformation, a bilinear plus nonlinear hardening model from Yun & Gardner (2017) is applied. As illustrated in Figure 4.2, the initial slope is linear and represents the elastic region of the material, limited by the yield stress. In this first stage, the steel is following Hooke's law, where stress is directly proportional to strain. This is followed by a section of plastic flow, creating a plateau with an almost constant stress, before reaching the strain hardening value. During the strain hardening phase, stress proceeds to accumulate until reaching the ultimate tensile stress, and the corresponding ultimate tensile strain.

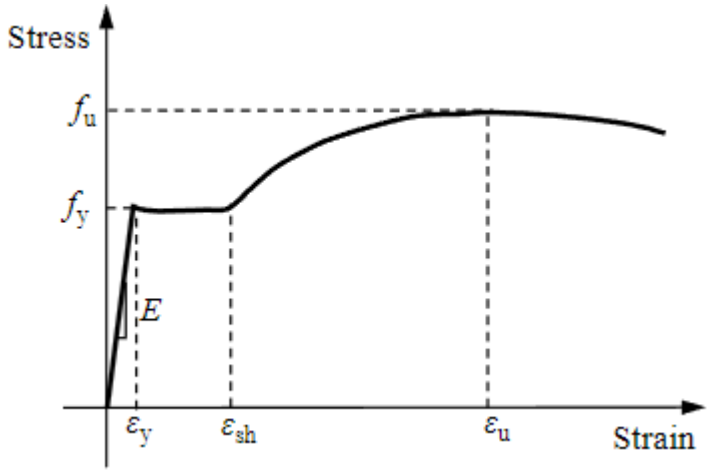

Figure 4.2: Bilinear plus nonlinear hardening model (Yun & Gardner, 2017)

The properties needed for the bilinear plus nonlinear hardening model is presented in Table 4.1 and Table 4.2. The web, reinforcement bars and flanges are calculated separately since the steel quality differs. The yield stress and ultimate stress are taken from Hällmark et al., (2021), the other parameters are calculated using said stresses. Numerical values are presented in table B.1.

Table 4.1: Input of elastic properties for steel

Property	Notation	Value
Poisson's ratio	v	0,3 -
Modulus of elasticity	E_s	210 GPa

Table 4.2: Input of plastic properties for steel

Property	Notation	Web	Flanges
Yield stress	f_y	447 MPa	407 MPa
Ultimate stress	f_u	579 MPa	541 MPa
Yield Strain	ε_y	0,002 -	0,002 -
Ultimate Strain	ε_u	0,137 -	0,149 -
Strain plastic	$\Delta\varepsilon$	0,135 -	0,147 -
Strain hardening	ε_{sh}	0,022 -	0,020 -

As established by Yun & Gardner (2017), the predictive expressions for ultimate strain and strain hardening in hot-rolled carbon steel are calculated using equations (4.1) and (4.2). Further on their proposed bilinear plus nonlinear material model for hot-rolled carbon steel is presented in equation (4.3), with the coefficients being proposed as $K_1 = 0{,}4$, $K_2 = 2$, $K_3 = 400$ and $K_4 = 5$.

Ultimate strain:

$$\varepsilon_u = 0{,}6 \cdot \left(1 - \frac{f_y}{f_u}\right) \tag{4.1}$$

Strain hardening:

$$\varepsilon_{sh} = 0{,}1 \cdot \frac{f_y}{f_u} - 0{,}055 \tag{4.2}$$

The stress is calculated with:

$$f(\varepsilon) = \begin{cases} E_\varepsilon \; for \; \varepsilon \leq \varepsilon_y \\ f_y \; for \; \varepsilon_y < \varepsilon < \varepsilon_{sh} \\ f_y + (f_u - f_y)\left\{ K_1 \left(\frac{\varepsilon - \varepsilon_{sh}}{\varepsilon_u - \varepsilon_{sh}}\right) + \frac{K_2 \left(\frac{\varepsilon - \varepsilon_{sh}}{\varepsilon_u - \varepsilon_{sh}}\right)}{\left[1 + K_3 \left(\frac{\varepsilon - \varepsilon_{sh}}{\varepsilon_u - \varepsilon_{sh}}\right)^{K_4}\right]^{\frac{1}{K_4}}} \right\} for \; \varepsilon_{sh} < \varepsilon \leq \varepsilon_u \end{cases} \tag{4.3}$$

For the rebars, the specified yield stress is approximate and the ultimate stress is unknown, thus no material tests were performed. In these calculations, an assumption is made that the rebars are delivered in exactly 500 MPa in yield strength. For ultimate strength, a rough estimation is made based on other material tests for quality B500B. Derived from the tests presented in Table B.2, a mean ultimate stress is obtained to 639 MPa.

4.2.2 Concrete

In the same way as for the steel, it is essential to define both the elastic and plastic behaviours of the concrete material. The Poisson's ratio for uncracked concrete is retrieved from EN-1992-1-1 (2005) and the modulus of elasticity is given in Hällmark et al., (2021), see Table 4.3.

Table 4.3: Input of elastic properties for concrete

Property	Notation	G1	G2
Poisson's ratio	v	0,2 -	0,2 -
Modulus of elasticity	E_{cm}	34,3 GPa	33,6 GPa

In Abaqus there is some different options to simulate inelastic material properties of reinforced concrete. In this case the concrete damaged plasticity method is chosen, as it has the potential to represent complete inelastic behaviour with damage characteristics (Wahalathantri et al., 2011).

The ratio of stress to strain is required input for the damaged concrete model. To get the most realistic result, data directly from cube tests would have been preferable. In this case however, the complete stress strain data was not available. It is still possible to produce reasonable data through computational models. In EN-1992-1-1 (2005) a formula for the relation between stress and strain in compression is presented, see equation (4.4).

$$\sigma_c = f_{cm} \frac{k\eta - \eta^2}{1+(k-2)\eta} \tag{4.4}$$

Where:

$$\eta = \frac{\varepsilon_c}{\varepsilon_{c1}} \tag{4.5}$$

Compressive strain in the concrete at the peak stress:

$$\varepsilon_{c1} = 0{,}7 \cdot {f_{cm}}^{0{,}31} \tag{4.6}$$

The factor k is calculated as:

$$k = \frac{1{,}05\, E_{cm} \cdot |\varepsilon_{c1}|}{f_{cm}} \tag{4.7}$$

The relation between stress and strain can be compiled according to the equation (4.4)–(4.7). This results in a ratio similar to the one presented in Figure 4.3, for exact numerical values for concrete stress – strain data see appendix B.

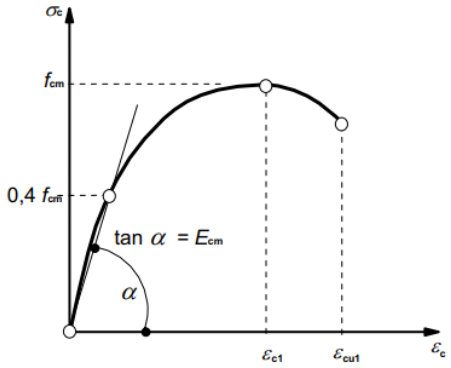

Figure 4.3: Stress-strain relation for structural analysis (SS-EN 1992-1-1, 2005)

Since concrete has different properties in compression and in tension, additional calculations are necessary to produce the required tensile properties. To describe tensile stress, a model from Nayal & Rasheed (2006) is used, see Figure 4.4.

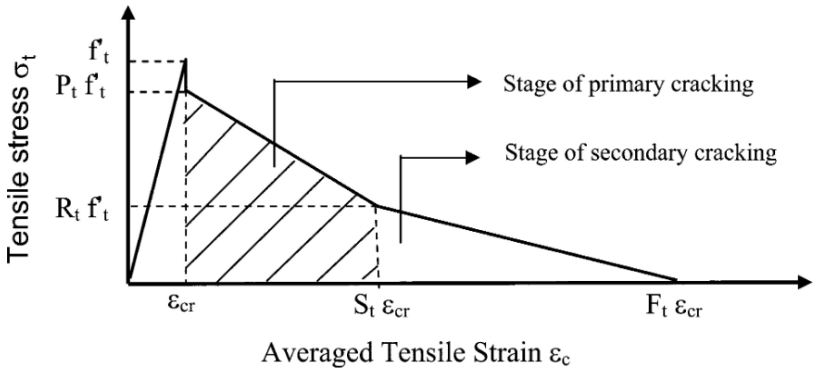

Figure 4.4: Model for tensile stress (Nayal & Rasheed, 2006)

The model presented in Figure 4.4 is then modified according to Wahalathantri et al., (2011), this is done to avoid run time errors. Figure 4.5 shows the selected tensile stress model.

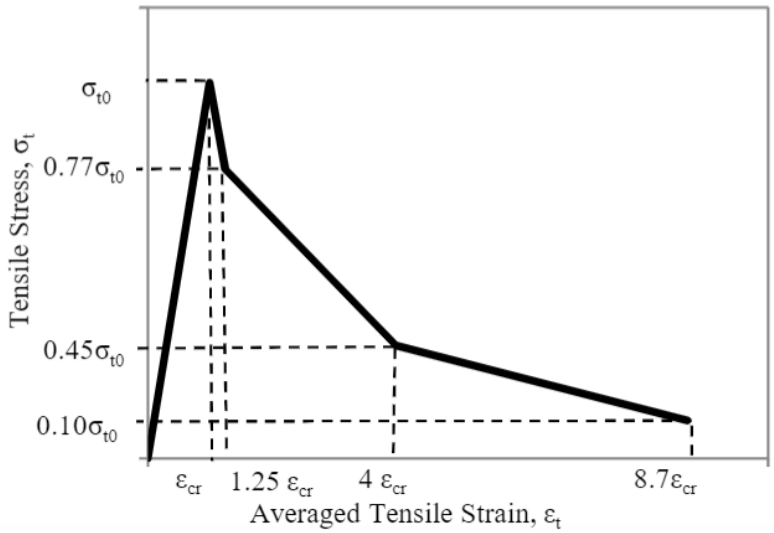

Figure 4.5: Tension stiffening model for Abaqus (Wahalathantri et al., 2011)

For each stress value provided, the corresponding strain must be entered. In Abaqus, the strain must be given in the form of inelastic strain (Dassault Systèmes, 2014). Except for the strain - stress data, a damage parameter must also be specified for the concrete damage plasticity model. This can be calculated as (Jankowiak & Lodygowski, 2005):

$$\sigma = (1 - d)\sigma_{cu} \qquad (4.8)$$

Extracts the damage parameter, d, from the equation (4.8):

$$d = 1 - \frac{\sigma}{\sigma_{cu}} \qquad (4.9)$$

The numerical values are presented in appendix B.

Five plasticity factors must be specified to define the material concrete. Since no material tests have been completed for the parameters, they are chosen according to the recommended values from Bilal et al., (2023). However, due to convergence issues, the viscosity parameter was changed in accordance with Demir et al., (2018), to a value of 0,0005 instead of 0. With this changes the models start working, but the execution was time consuming. Due to this problem the viscosity parameter was chosen as 0,01, see chapter 6.2 for extended analyse for the choose.

Table 4.4: Plasticity parameters

Dilation angle	Eccentricity	fb_0/fc_0	K	Viscosity parameter
38	0,1	1,16	0,667	0,01

4.2.3 Coiled spring pins

Data for the CSPs properties was provided from the CSP push-out tests presented in Hällmark et al., (2019). The tests were conducted on a test set up consisting of two steel plates with a concrete box between, connected with the CSPs. To obtain the material properties for the connectors, a load plate is added to push the concrete and steel apart, see Figure 4.6.

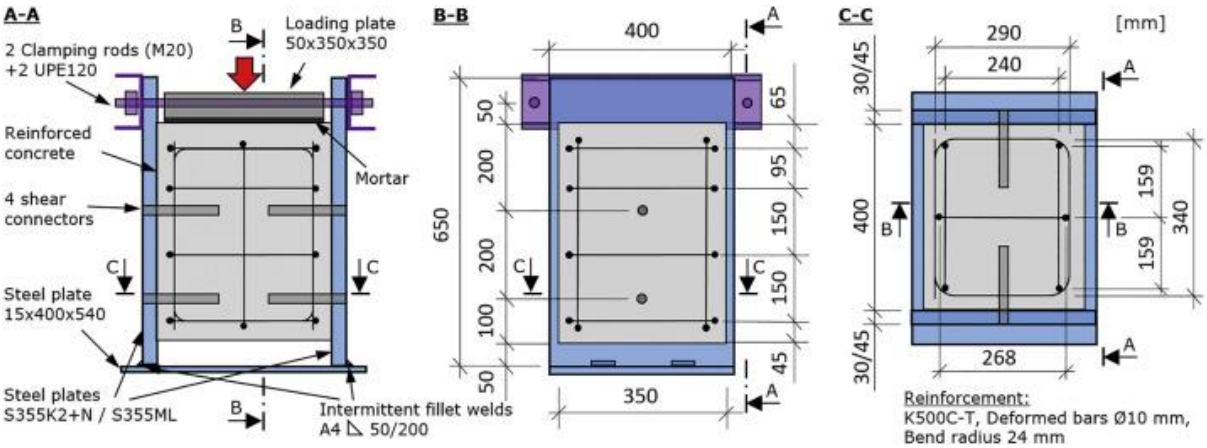

Figure 4.6: Test set up for CSP's material properties (Hällmark et al., 2019)

The provided data from the push-out tests is presented in Figure 4.7. This data is used as input for the modelled springs, that represent the CSP's.

Figure 4.7: Provided data for coiled spring pins (Hällmark et al., 2019)

4.3 Boundary conditions and interactions

The supports were defined as lines positioned 200 mm inwards from each end of the girder, beneath the bottom flange. Their boundary conditions are fixed except for translation along the beam and rotation around the supports.

Two different methods are used to describe the properties of the beam under load. For the first method a boundary condition is applied on the load plate, all degrees of freedom are set as fixed except for displacement downwards. This method is used for testing different models, thus it proved to reduce the run time compared to applying the loads directly. When the model is considered correct, method two is used instead. Method two is simply applying a point load to a reference point in the centre of the load plate instead of using displacement. In order to distribute the stresses in the contact surface between the concrete deck and the load plate, the reference point was connected to the load plate with the tool coupling constrains. The constraint connects a reference node with a surface of nodes, which in this case means that the point load is connected to the entire load plate surface and the load is therefore distributed over the plate (Dassault Systèmes, 2014).

To describe the behaviour of the girders, it is necessary to define the properties of all interaction surfaces. For the test beams there are mainly three major interactions, between load plate and concrete deck, concrete deck and steel beam and between the supports and the girder. Since there are no material tests provided for the friction coefficients, reasonable values are assumed to get FEM results close to the laboratory tests. For the surfaces between steel and concrete, a friction coefficient of 0,377 is used based on the tests presented in Guo et al., (2020). No friction coefficient is added for the contact surface between supports and the steel girder, this is done to simplify the model as no separate supports were created.

To get the stiffeners to interact with the steel girder in a way that replicates the properties of the welds, they are connected to the girder using the constraint tie command. The command connects two surfaces so there is no relative motion between them, in this case there is no motion between the stiffeners and the steel flanges (Dassault Systèmes, 2014).

The embedded region constraint is applied to ensure that the reinforcement bars are kept in place by the surrounding concrete. The command embeds the steel reinforcement in a host region, restricting it from movement and thereby contribute to a more realistic simulation (Dassault Systèmes, 2014).

4.4 Mesh sensitivity

Applying a proper mesh to the model is essential to acquire a more precise result and reduce the risk of having convergence issues (Ansys, 2021). While a finer mesh generally contributes to a more accurate result, the computation time increases. Achieving a mesh that effectively balances accuracy and computational resources can be done using a mesh convergence study. The mesh convergence study can be divided into two steps:

- Generate a mesh using the minimum reasonable number of elements.
- Increase the mesh density by decreasing the element size and regenerate the mesh.

Compare the results to those of the previous mesh and keep repeating the steps until a satisfactory element size is attained (Autodesk, 2023).

The steps were reiterated until the difference between the stresses from the result was less than 1%. The outcome of the mesh convergence study can be seen in Table 4.5, thus no significant difference in maximum stress was obtained between the attempts, no further test was completed. The mesh presented in the second attempt is chosen for all Abaqus models, an illustration of the mesh can be seen in Figure 4.8:

Table 4.5: Convergency study outcome for full composite action

Part	Element size	
Concrete deck	60	50
Steel beam	60	50
Reinforcement-AΦ12	50	30
Reinforcement-AΦ16	50	30
Reinforcement-NΦ12	50	30
Load plate	50	30
Stiffener	50	30
Maximum stress [MPa]	156,0	156,6

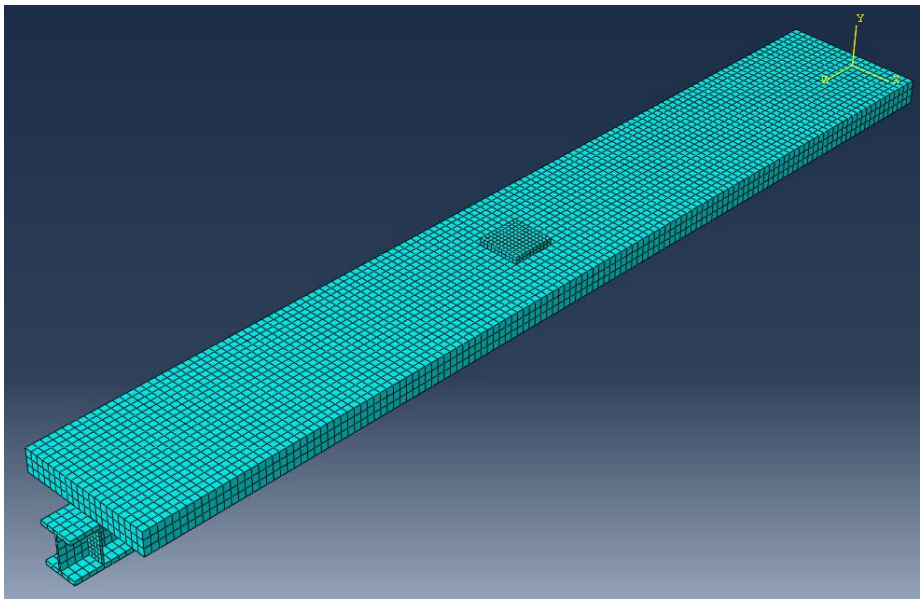

Figure 4.8: Illustration of selected mesh

5 Hand calculations

To validate the results obtained through the FEM-analysis, simple and approximative hand calculations have been conducted. The calculations are done according to the book Isaksson & Mårtensson (2019), that is condensed version of the Eurocodes. The results from the hand calculations are then compared to evaluate if the stresses and displacements are reasonable compared to the other methods.

The assumption is made that the web takes all the load, without considering the contributions of the stiffeners. Extensive calculations and tables are presented in appendix C.

5.1 Cross-section classification

The web and flanges of rolled steel sections are relatively slender in relation to their length and width, which may require checks for local buckling depending on the cross-section class they are categorised in. The web and flange can belong to different classes, classified according to the highest cross-section class for the compressed parts. For this steel profile, the cross-section class is determined as CS class 1 for both the flange and web, and no check for local buckling needs to be carried out.

5.2 Moment of inertia

The moment of inertia is calculated according to the parallel axis theorem (Isaksson & Mårtensson, 2019):

$$I_y = I_{yi} + A_i e_i^2 \tag{5.1}$$

Each part's moment of inertia:

$$I_{yi} = \frac{wh^3}{12} \tag{5.2}$$

Calculations for moment of inertia are divided into two parts, one without composite action and the other with composite action. When doing calculations without composite action, the moment of inertia is calculated for each part separately, i.e., the concrete deck and steel girder individually. When considering full composite action, a common centre of gravity is used treating the two parts as one specimen. Furthermore, since it's a composite beam the concrete is transformed into steel to be able to summarise the two moments of inertia. This is done using the transformed section method, meaning that the moment of inertia for the concrete is multiplied by the ratio between the two materials moduli of elasticity (Collin et al., 2012).

5.3 Calculation of stresses and displacements

The results from the hand calculations are presented in form of stresses and displacements. The general equations to do the calculations are presented equation (5.3) and (5.4), numerical values and complete approach is presented in appendix C.

Maximum displacement for a simply supported beam:

$$U_{max} = \frac{FL^3}{48EI} \tag{5.3}$$

Stress from bending moment:

$$\sigma = \frac{M \cdot e}{I} \tag{5.4}$$

For the calculations of stress and displacement, in case of non-composite action girder, the distribution of load on each part must be specified. Since no further analyses have been carried out regarding the distribution, it is assumed that the load is distributed according to the different moduli of elasticity for the two materials. For the calculation of full composite action, the principle with a common centre of gravity is used, in the same way as previously calculations for full composite action.

6 Factors that may impact the accuracy of the FEM simulations

The FEM simulations presented in chapter 4 aim to replicate the behaviours exhibited by an actual girder. Although the model has been implemented with high accuracy, some deviation is expected due to uncertain factors. For these factors, no tests have been conducted and the values are chosen from literature. The impact from the factors is therefore important to study, as they can affect the models.

The identified factors are:

- Friction coefficient
- Dilation Angle
- Viscosity parameter

6.1 Friction coefficient between steel and concrete

The friction coefficient can be hard to determine as it depends on factors as roughness, surface hardness and the crack resistance of concrete (Guo et al., 2020). To get an accurate friction coefficient, friction force tests would be preferable. However, as the tests can be time ineffective an evaluation is done to consider the accuracy of approximations for the coefficient.

To evaluate the friction coefficients impact on a girder, a minor analytical test is created in Abaqus. The test compares the maximum stress and displacement for different friction coefficients, the stresses are measured in accordance to Figure 6.1. Girder 1, with non-composite action, is used as test beam with a subjected point load of 350 kN. Since only the difference of the maximum values is of importance in this chapter, the materials are simplified to having only elastic properties to reduce the run time. From the results presented in Table 6.1, a difference of 2.4 MPa is shown between the extreme cases.

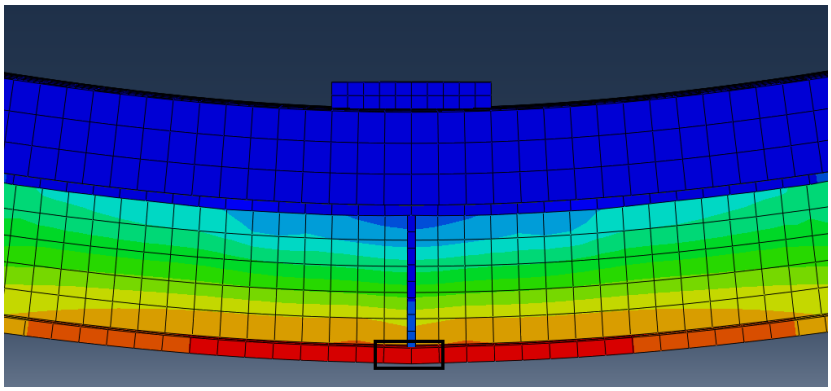

Figure 6.1: Measuring location for stresses

Table 6.1: Maximum stress and displacement for different friction coefficients, F=350 kN

μ	$\sigma_{l.f}$ [MPa]	U [mm]
0,6	193,5	27,2
0,5	194	27,3
0,4	194,5	27,4
0,377	194,6	27,4
0,3	195	27,5
0,2	195,5	27,6
0,1	195,9	27,7

Further test is compiled to verify the friction impact for FEM simulations of composite girders on a more general way. Two factors are identified to possibly influence the friction behaviour, the material stiffness and the distribution of the load acting on a girder.

To evaluate if the friction coefficient is more sensitive for different stiffnesses, a new minor analysis is conducted, see Table 6.2. The same beam is used as before, but with varied values of modulus of elasticity.

Table 6.2: The friction coefficient impact for different modulus of elasticity, F=350 kN

E [GPa]	μ	$\sigma_{1.f}$ [MPa]	U [mm]	$\sigma_{2,1.f}/\sigma_{1,1.f}$	U_2/U_1
37	0,6	190,6	26,8	1,0121	1,0187
	0,1	192,9	27,3		
34,3	0,6	193,5	27,2	1,0124	1,0184
	0,1	195,9	27,7		
27	0,6	202	28,4	1,0129	1,0176
	0,1	204,6	28,9		

In the previous simulations, the load is applied over the load plate in the centre of the beam. However, to analyse if the distribution of the load affects the friction coefficient a new minor test is conducted. The test compares the difference between the ordinary beam and a beam with the load distributed in three points, one in 1/3, 1/2 and 2/3 of the beam length, see Figure 6.2.The test is conducted because an arch effect occurred between steel beam and concrete deck for the non-composite versions in FEM, this effect is presented further in the result chapter. For this model's complete plastic material properties is used for the concrete, thus the arch effect does not appear for elastic material behaviour. The friction impact ratio for both the stresses and displacements increases with the alternative with three loads, see the results in Table 6.3.

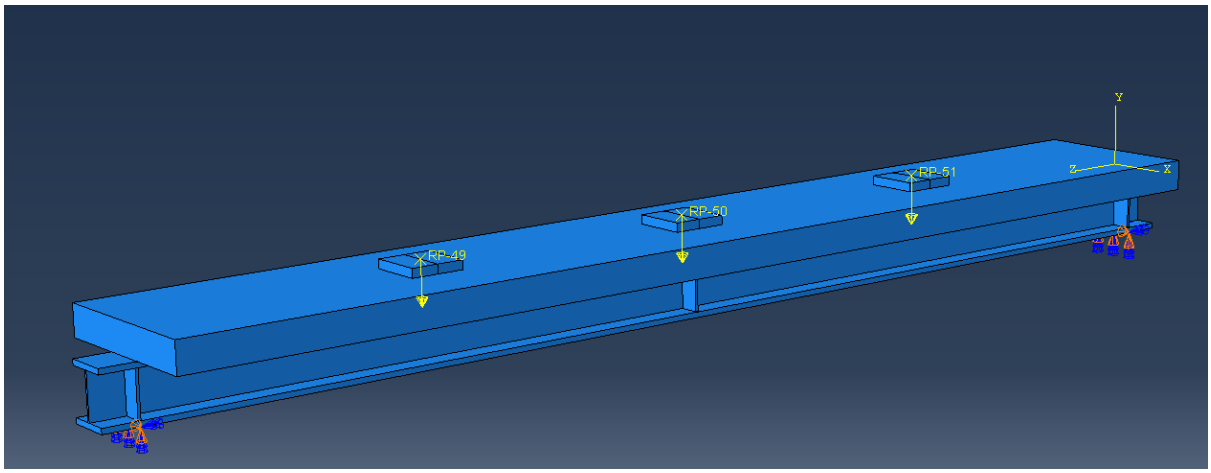

Figure 6.2: Illustration of loads subjected to the beam

Table 6.3: The load distributions impact for different friction values, F=350 kN

Load distribution	μ	$\sigma_{1.f}$ [MPa]	U [mm]	$\sigma_{2,1.f}/\sigma_{1,1.f}$	U_2/U_1
Central load	0,6	230	31,8	1,011	1,009
Central load	0,1	232,5	32,1		
3 point loads	0,6	151,3	23,4	1,036	1,051
3 point loads	0,1	156,7	24,6		

For partial composite action, one minor test is conducted to evaluate the sensitivity of the friction coefficient, the results are presented in Table 6.4

Table 6.4: Maximum stress and displacement for different friction coefficients, F=350 kN

μ	$\sigma_{l.f}$ [MPa]	U [mm]
0,6	167,7	13,0
0,377	168,4	13,0
0,1	169,3	13,0

6.2 Viscosity parameter

By default, Abaqus sets the viscosity parameter to zero. However, following Dassault Systèmes (2014) suggestion, introducing a small nonzero value to the viscosity parameter usually aids in resolving convergence issues of the model, without compromising the accuracy of the results.

A minor numerical study was conducted to investigate the sensitivity of the viscosity parameter. Four different values were tested on Girder 2 subjected to a point load of 350 kN, evaluating the accuracy of the stresses as well as the time to complete the simulations. As seen in Table 6.5 the simulation time increases drastically when the viscosity parameter decreases.

Table 6.5: Impact of viscosity parameter value on Girder 2 with non-composite action, F=350 kN

Input	Time of simulation	$\sigma_{l.f}$ [MPa]	$\sigma_{u.f}$ [MPa]	$\sigma_{t.c}$ [MPa]
0,0005	1 h	234,2	-229,7	-12,9
0,001	45 min 40 sec	234,3	-229,7	-13,1
0,01	9 min 50 sec	233,5	-228,4	-13,9
0,1	3 min 34 sec	226,1	-220,5	-16,5
1	1 min 39 sec	206,7	-200,2	-18,4

6.3 Dilation angle

The dilation angle is by literature described as a crucial component of the CDP model for obtaining realistic simulation results. When concrete is affected by inelastic strains it experiences substantial alterations in volume, this is referred to as dilatancy (Bilal et al., 2023; Jabbar, M. A., 2023). A sensitivity analysis is performed to evaluate the impact of the dilation angle on Girder 2 subjected to a point load of 350 kN, and the results are presented in Table 6.6.

Table 6.6: Impact of the dilation angle parameter value on Girder 2 with non-composite action, F=350 kN

Input	$\sigma_{l.f}$ [MPa]
10	231,2
20	231,4
30	231,2
40	231,0
50	230,3

7 Laboratory tests

All the numerical values in chapter 7 are based on a compilation of the laboratory test presented by Robert Hällmark (Personal communication).

In the laboratory test, five gauges were used for strain, two wire sensors for displacement and one LVDT sensor were used for measurement of slip. The gauges are numbered 1-5 with the first placed at the top and the last in the bottom flange, the setup is presented in Figure 7.1. As the different measurement tools were used for all the loads presented in chapter 3.5, an extensive result file was provided. However, to get a reasonable amount of data to analyse, only data for girders subjected to a load of 350 kN and 870 kN is presented. Four cases are included, Girder 1 and Girder 2 and both with values for non-composite action and partial composite action.

The displacement is measured in two separate wires, this is done to verify that the girder is not subjected to lateral torsional buckling or another type of non-vertical displacement. Both the measurements for displacement and strain presents mid span values, thus it is the location of the expected maximum values. For the slip the measurements are done over the supports, one measurement for each support.

Between the load cycles there were inconsistencies regarding zeroing of the strain, this means that for some cases the results will be deviating.

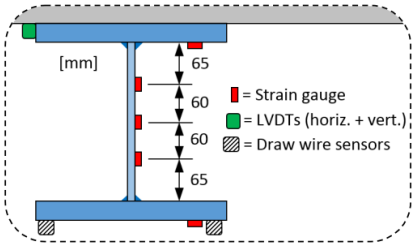

Figure 7.1: Measurement tools, figure provided from Rober Hällmark (2021)

7.1 Data for Girder 1 with non-composite action

Displacement, strain and slip for Girder 1 is presented in Figure 7.2, Figure 7.3, and Figure 7.4. The girder in this case is subjected to the load of 350 kN with no shear connectors added. In the end of the curve in Figure 7.4, the slip does not change even if the load increases for LVDT B. The reason for this deviation is assumed to depend on the LVDT sensor reaching its maximum position. Due to this, the results for the slip in support B should be considered with caution. Between the load cycles the strain is inconsistent set to zero, to account for this, the initial strain value is subtracted for the results in chapter 8.3.

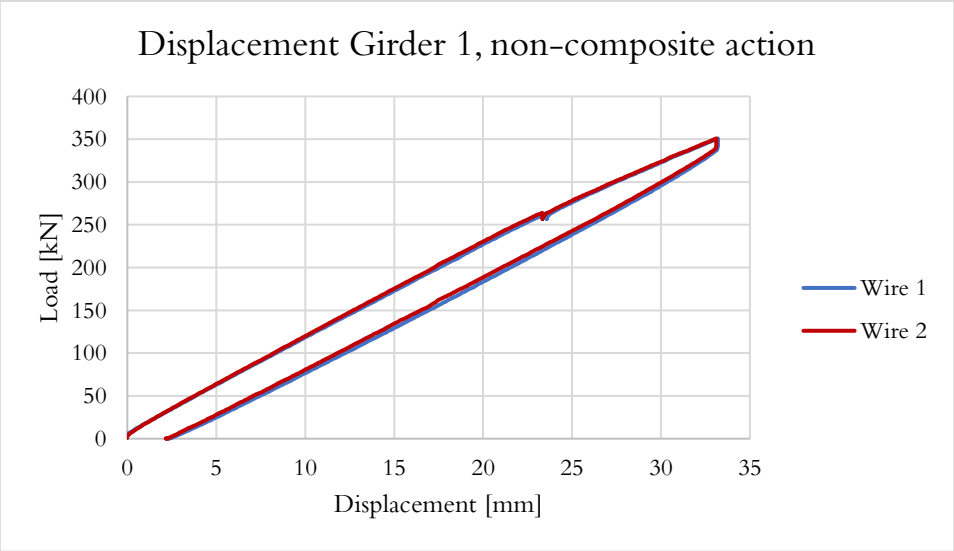

Figure 7.2: Measured displacement for Girder 1 with non-composite action

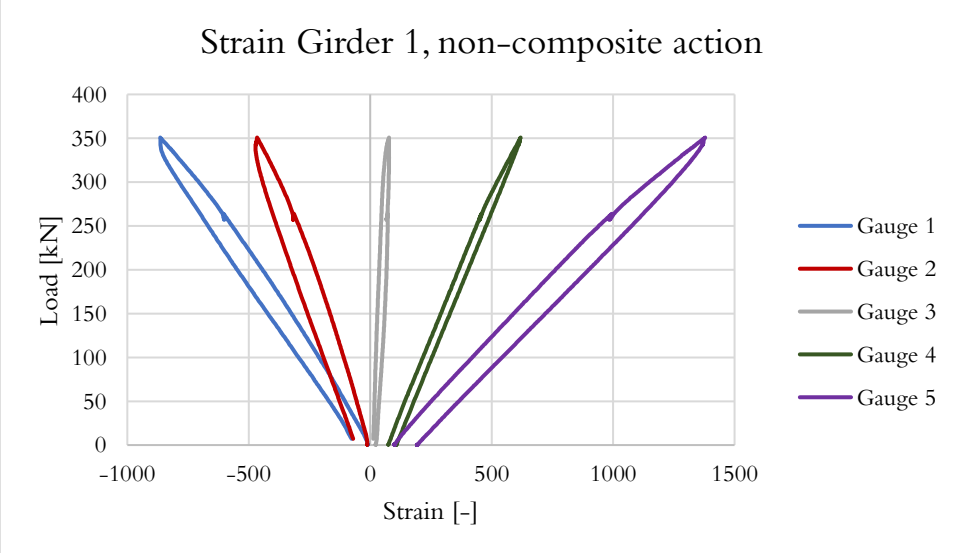

Figure 7.3: Measured strain for Girder 1 with non-composite action

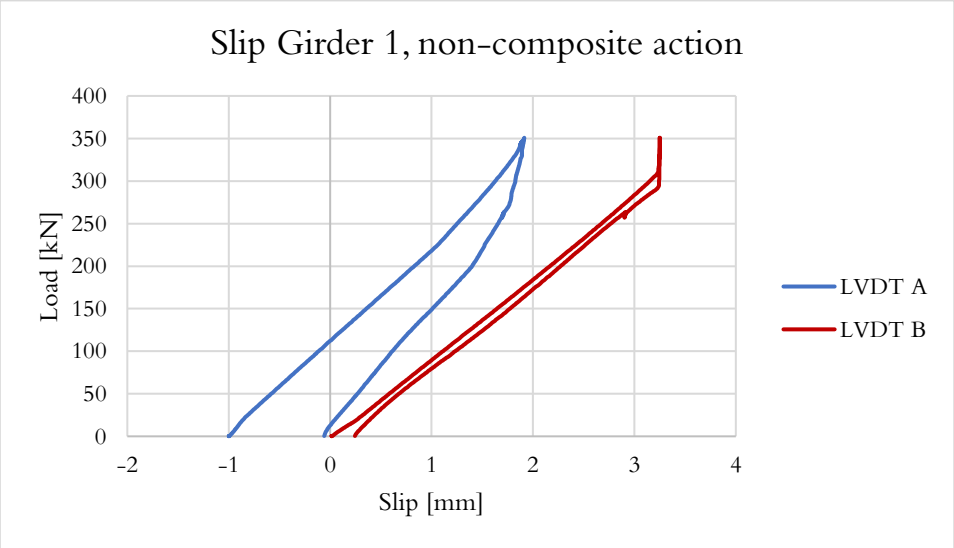

Figure 7.4: Measured slip for Girder 1 with non-composite action

7.2 Data for Girder 2 with non-composite action

For Girder 2, data for displacement, strain and slip is presented in Figure 7.5, Figure 7.6, and Figure 7.7. The provided difference between Girder 1 and 2 is that the concrete in Girder 2 has a slightly lower strength. However, for this tests Girder 2 proved to have less displacement and lower stresses although it has lower strength. One possible explanation for the unexpected results, could be the difference in slip between the two girders. A clear slip occurs on Girder 1 in both supports, for Girder 2 there is almost no slip at support B. As mentioned in chapter 2.1.2, a near zero slip means that the layers in the structure acts as a component and therefore reaches a sort of partial composite action. Due to this, Girder 2 is expected to still have a sort of partial composite action unlike Girder 1.

Between the load cycles the strain is inconsistent set to zero, to account for this, the initial strain value is subtracted for the results in chapter 8.3.

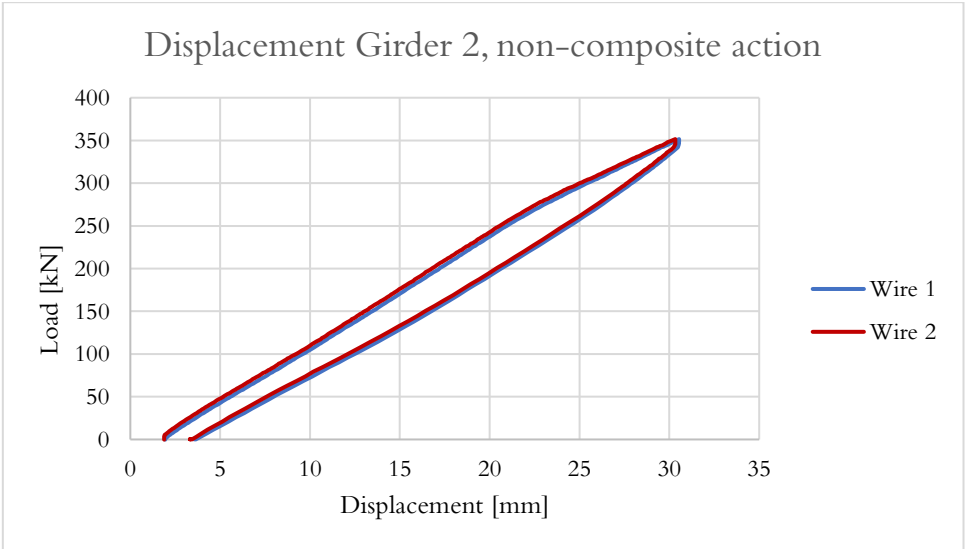

Figure 7.5: Measured displacement for Girder 2 with non-composite action

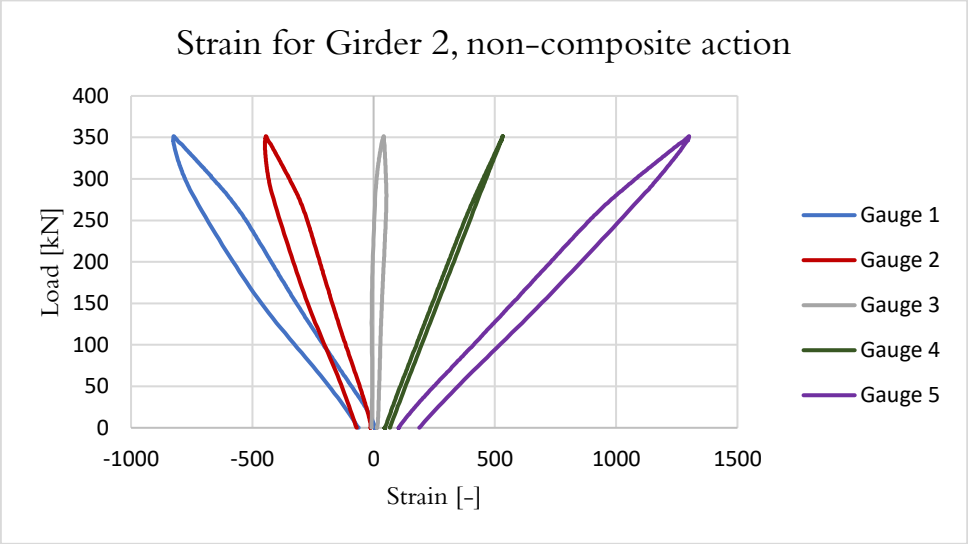

Figure 7.6: Measured strain for Girder 2 with non-composite action

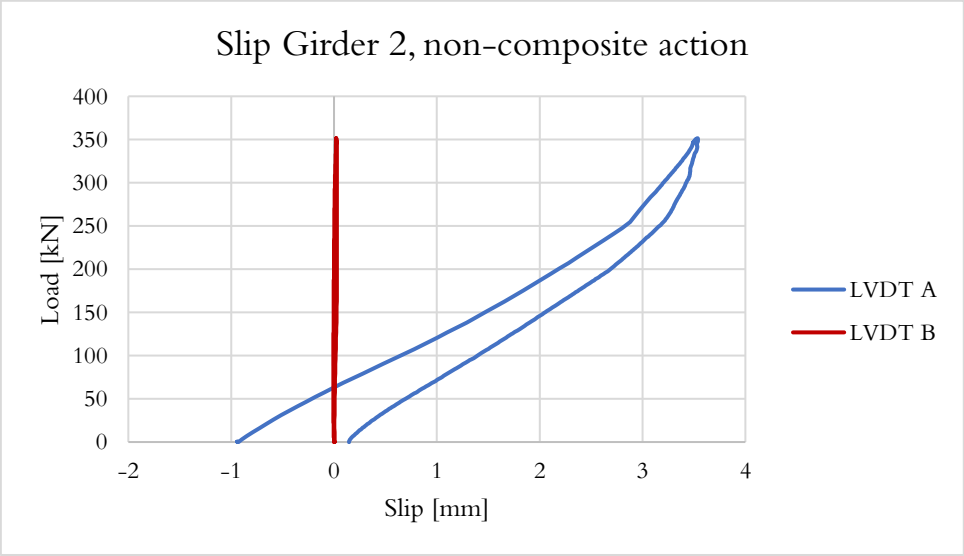

Figure 7.7: Measured slip for Girder 2 with non-composite action

7.3 Data for Girder 1 with partial composite action

For this case, coiled spring pins were placed evenly distributed in six pairs from each side on Girder 1, accordance to Figure 3.4. The data from the laboratory tests is presented in Figure 7.8, Figure 7.9, and Figure 7.10. As expected, the shear connectors improved the strength of the girder in the test.

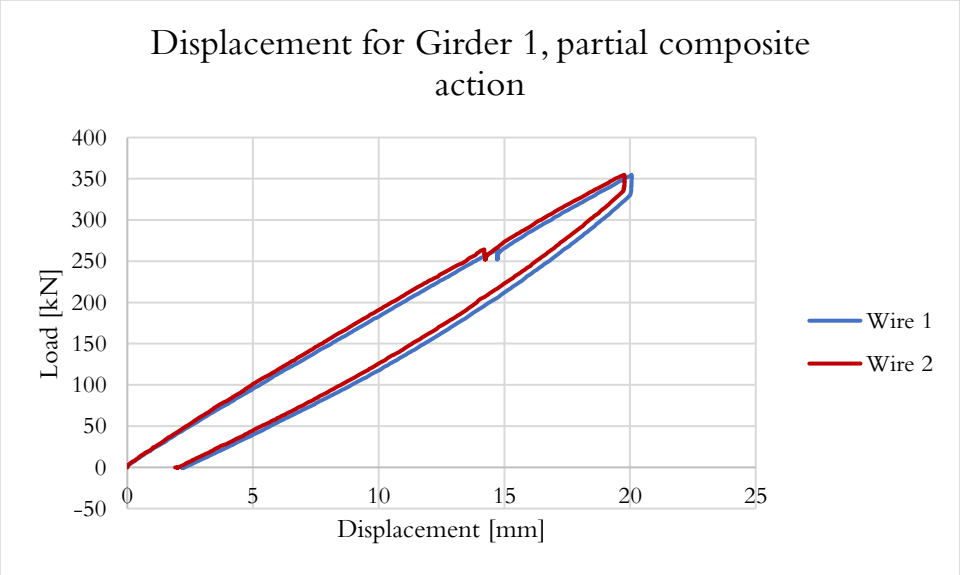

Figure 7.8: Measured displacement for Girder 1 with partial composite action

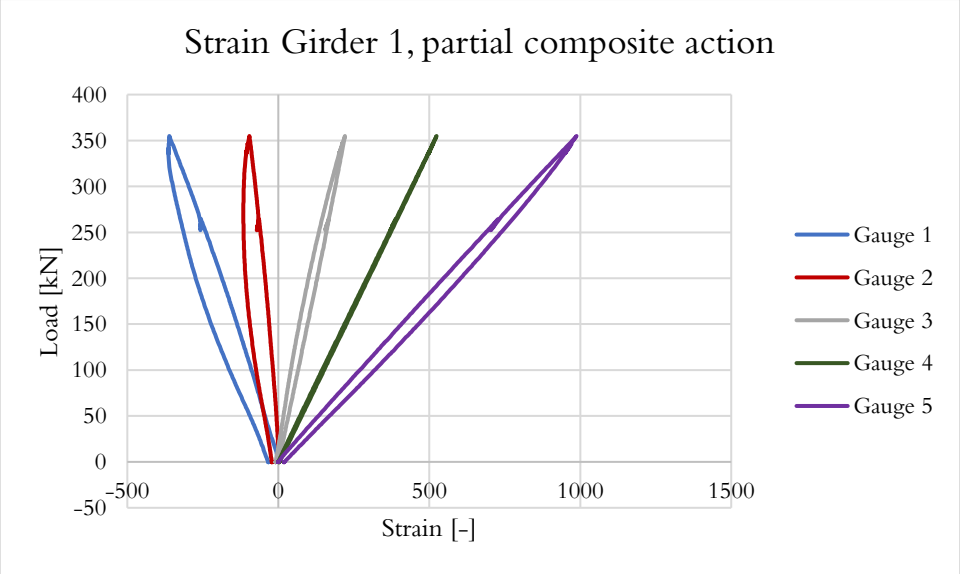

Figure 7.9: Measured strain for Girder 1 with partial composite action

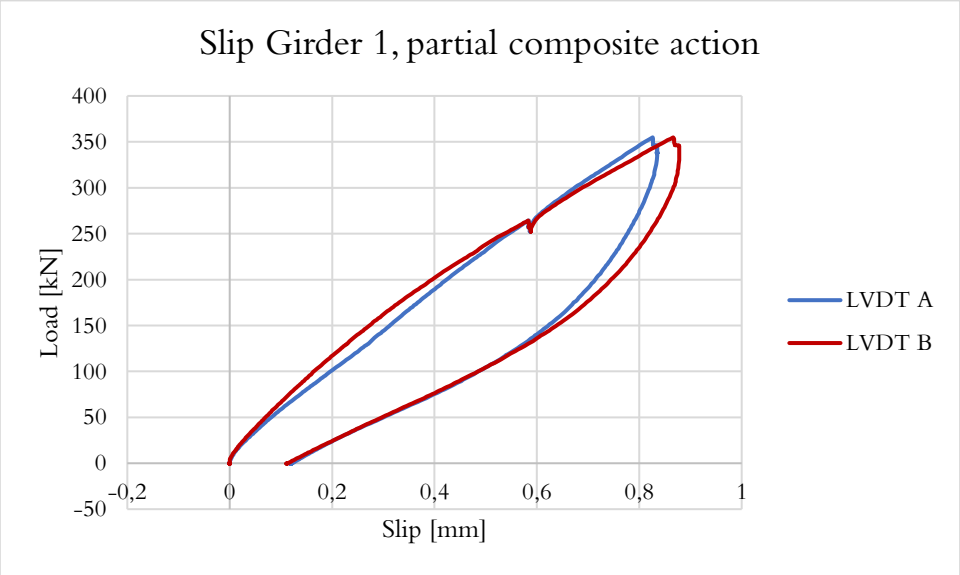

Figure 7.10: Measured slip for Girder 1 with partial composite action

7.4 Data for Girder 2 with partial composite action

Girder 2 is strengthened with an equal number of CSPs as Girder 1. However, the placement of the CSPs is different as they are placed in a zigzag pattern where the first eight connectors have a cc distance of 180 mm, and the last four have a cc distance of 360 mm, see Figure 3.5. The result from the tests is presented in Figure 7.11, Figure 7.12, and Figure 7.13. In the same way as Girder 1, did the CSPs improve the strength of the girder. For the first two cases with non-composite action, Girder 2 had lower displacement and lower stresses. As the CSPs are implemented, this ratio changes and Girder 1 gets lower displacements and stresses. Whether this is a consequence of the placements of the CSPs, or some other factor is difficult to establish.

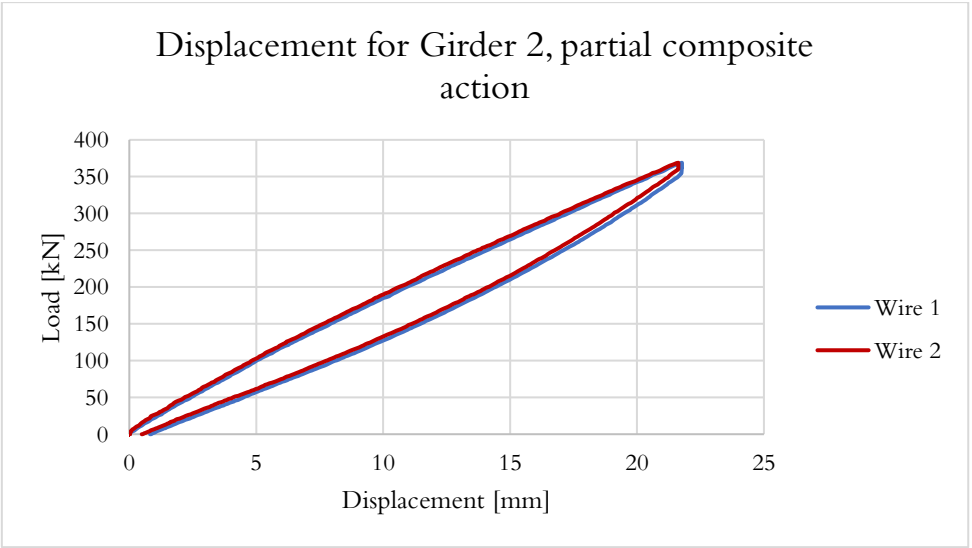

Figure 7.11: Measured displacement for Girder 2 with partial composite action

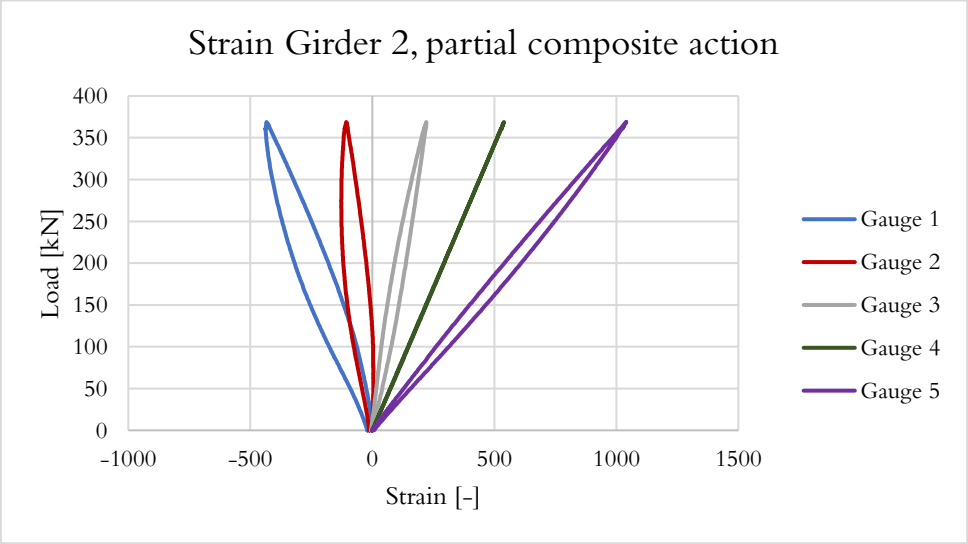

Figure 7.12: Measured strain for Girder 2 with partial composite action

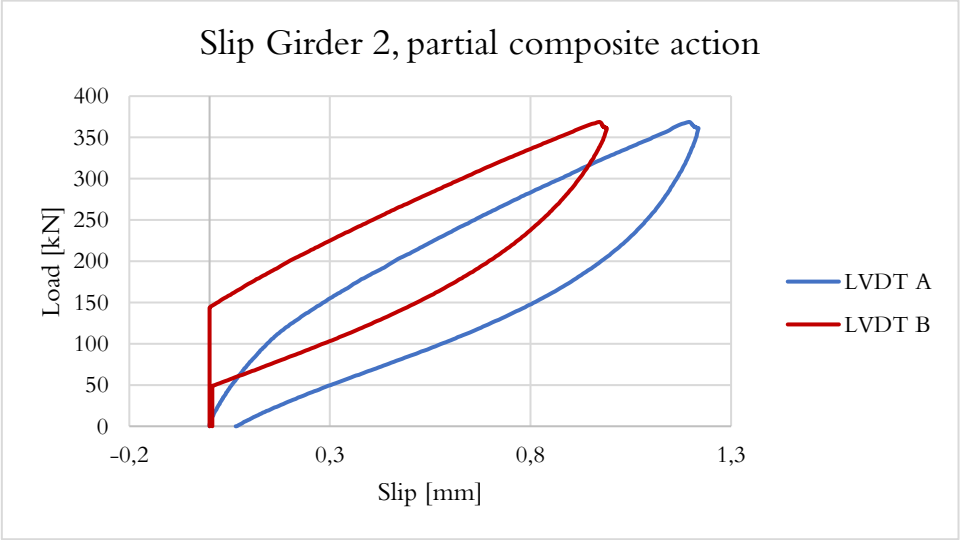

Figure 7.13: Measured strain for Girder 2 with partial composite action

7.5 Displacement for high loads

The intention was to load each girder to failure. However, as previously mentioned, the test concluded prematurely upon reaching a load of 870 kN. This unexpected limitation occurred when the girder contacted the floor, halting further deformation. Consequently, Figure 7.14 and Figure 7.15 below do not depict the beams reaching their failure point, but rather indicate when their deformation was physically halted by the floor. This is the reason behind the seemingly vertical lines.

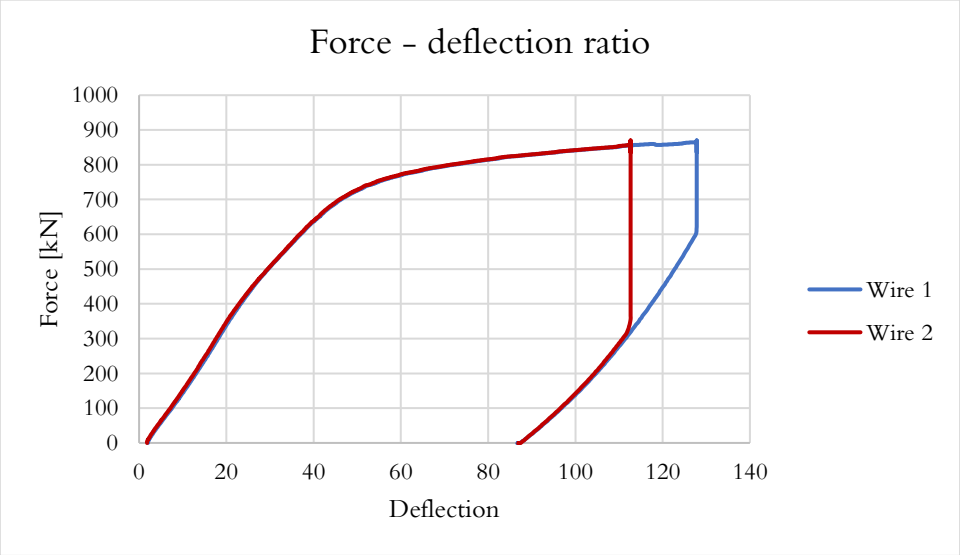

Figure 7.14: Girder 1 subjected to a load of 870 kN

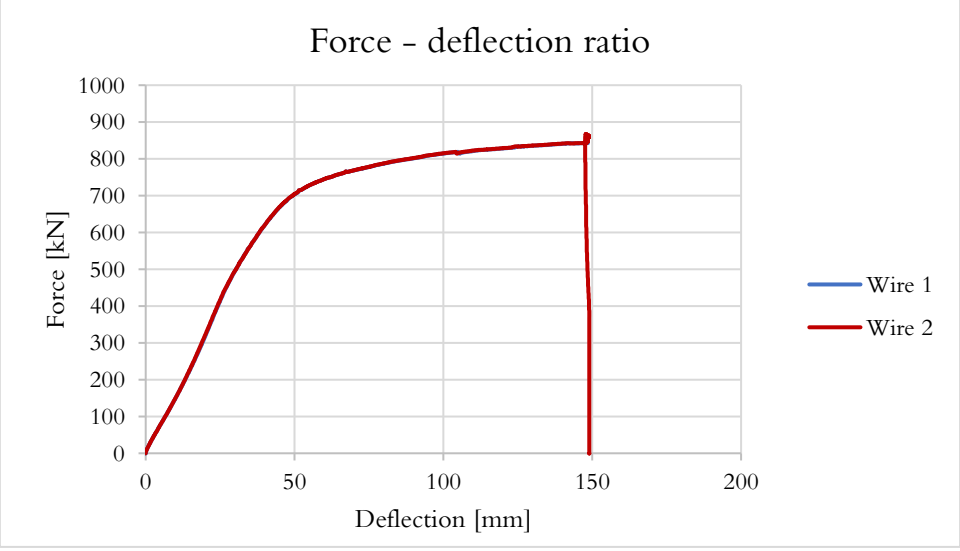

Figure 7.15: Girder 2 subjected to a load of 870 kN

8 Results

8.1 Hand calculations

Two distinct types of hand calculations were performed within Excel: one for the girder with non-composite action and a second for full composite action. Both calculations were made with a point load of 350 kN. Stresses were calculated at specific points of the beam including:

- Top of the concrete deck
- Top of upper flange
- Bottom upper flange
- Middle of web
- Top of lower flange
- Bottom lower flange

The stresses are presented in Table 8.1 and

Table 8.3. This is followed by Table 8.4 and Table 8.5 that showcases the maximum displacement calculated for each case. For non-composite action the displacement is computed separately for the steel and concrete due to simplification of the calculations. An additional calculation is presented in Table 8.2 and Table 8.6, this showcases the non-composite version with no acting concrete.

Table 8.1: Hand calculated stresses for non-composite action, F=350 kN

Notation	G1 [MPa]	G2 [MPa]
$\sigma_{t.c}$	-20	-19
$\sigma_{t.u.f}$	-241	-242
$\sigma_{b.u.f}$	-218	-219
σ_{w}	0	0
$\sigma_{t.l.f}$	218	219
$\sigma_{b.l.f}$	241	242

Table 8.2: Hand calculated stresses for non-composite action, only acting steel, F=350 kN

Notation	G1 [MPa]	G2 [MPa]
$\sigma_{l.f}$	288	288

Table 8.3 Hand calculated stresses for full composite action, F=350 kN

Notation	G1 [MPa]	G2 [MPa]
$\sigma_{t.c}$	-103	-104
$\sigma_{t.u.f}$	-5	-6
$\sigma_{b.u.f}$	12	11
σ_{w}	84	83
$\sigma_{t.l.f}$	155	156
$\sigma_{b.l.f}$	172	173

Table 8.4: Hand calculated maximum displacements for non-composite action, F=350 kN

Notation	G1 [mm]	G2 [mm]
U_{steel}	28,9	29,0
$U_{concrete}$	24,4	24,4

Table 8.5: Hand calculated maximum displacements for full composite action, F=350 kN

Notation	G1 [mm]	G2 [mm]
U_{FC}	9,9	10

Table 8.6: Hand calculated maximum displacements for non-composite action, only acting steel, F=350 kN

Notation	G1 [mm]	G2 [mm]
U_{steel}	32,1	32,1

8.2 FEM simulations in Abaqus

Three distinct types of FEM models were generated within the Abaqus software: one for the girder with non-composite action, a second for full composite action, and a third for partial composite action. For the models without coiled spring pins, an arch effect appeared for the lower loads, see Figure 8.1. This resulted in a gap between the concrete deck and the steel beam that affects the behaviour of the girder. However, this gap was reduced to zero as CSPs were added for the partial composite model.

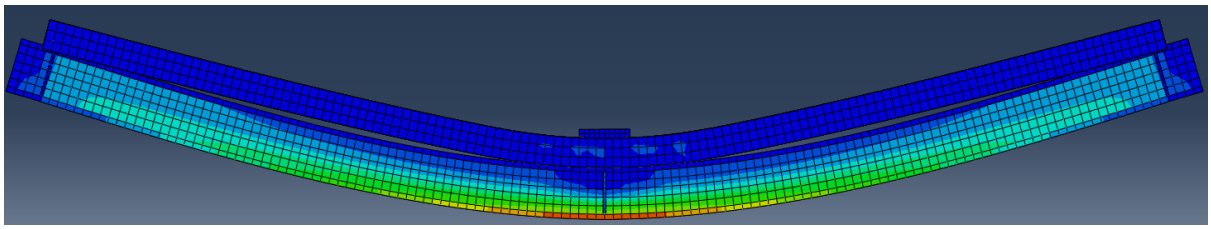

Figure 8.1: Arch effect between concrete deck and steel girder, with a subjected load of 350 kN

The concrete deforms elastically until the tenision limit state is reached, see Figure 4.4 and Figure 4.5. After a load of 80 kN, the concrete started to be utilized close to the tension limit state and plastic strain started to occur. For 200 kN this strain had increased significantly and resulted in tension values that has exceeded the tension limit for the concrete. The grey zones in Figure 8.2 indicates plastic strain and possibly cracks at the bottom of the concrete.

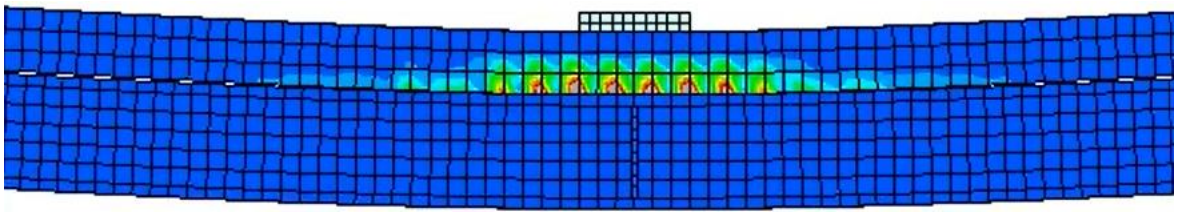

Figure 8.2: Strain in G2 for a load of 200kN. Grey zone indicates plastic strain

8.2.1 FEM simulations for stresses and displacements

Stresses were measured at specific points of the middle of the beam including: the top of the concrete deck, the upper flange, the midsection of the web, and the bottom flange. The stresses are presented in Table 8.7, Table 8.8 and Table 8.9 below and the placement of the CPSs are defined in chapter 3.4. This is followed by Table 8.10 that showcases the maximum displacement observed for each individual case. The results presented in the tables below are based on models subjected to a point load of 350 kN.

Table 8.7: Simulated stresses for non-composite action, F=350 kN

Notation	G1 [MPa]	G2 [MPa]
$\sigma_{t.c}$	-12	-13
$\sigma_{u.f}$	-224	-225
σ_{w}	-15	-17
$\sigma_{l.f}$	231	231

Table 8.8: Simulated stresses for full composite action, F=350 kN

Notation	G1 [MPa]	G2 [MPa]
$\sigma_{t.c}$	-16	-16
$\sigma_{u.f}$	15	14
σ_{w}	77	77
$\sigma_{l.f}$	150	150

Table 8.9: Simulated stresses for partial composite action, F=350 kN

Notation	G1 [MPa]	G2 [MPa]
$\sigma_{t.c}$	-18	-17
$\sigma_{u.f}$	-60	-18
σ_{w}	49	65
$\sigma_{l.f}$	168	156

Table 8.10: Simulated maximum displacement of the girders, F=350 kN

Notation	G1 [mm]	G2 [mm]
U_{NC}	31,9	32,6
U_{FC}	10,8	10,9
U_{PC}	13,0	11,9

8.2.2 FEM simulations for slip

To verify whether the models behave as the conducted tests, data for the slip between the concrete deck and the steel beam is analysed. The result for the slip is presented in Table 8.11.

Table 8.11: Simulated slip for non-composite action, F=350 kN

Notations	G1 [mm]		G2 [mm]	
	A	B	A	B
δ_{NC}	3,5	3,5	3,5	3,5
δ_{FC}	0,03	0,03	0,03	0,03
δ_{PC}	0,06	0,06	0,14	0,11

8.3 Comparison between calculations, simulations, and laboratory tests

8.3.1 Comparison between stresses

A comparison between the stresses in the lower flange, from the different calculation methods, is presented in Table 8.12, Table 8.13, and Table 8.14. The stresses are calculated for a load of 350 kN in Table 8.12 and Table 8.14. In Table 8.13 the full composite action versions of hand calculations and simulations is compared to the laboratory test, non-composite version, with the load of 150 kN. The lower load is used to replicate the behaviour of full composite action in the laboratory test, as the slip was expected to be small. Exact measurement points vary between the different methods. The hand calculations give values for middle part of flanges instead of values further out on the flanges, that is the case for the other calculations. The measurements from the FEM simulations and the laboratory test are not either completely comparable, thus the FEM simulations show the maximum value in a zone of values instead of the specific value given in the laboratory test.

Table 8.12: Comparison of stresses in lower flange with non-composite action, F=350 kN

Method	G1 [MPa]	G2 [MPa]
Hand calculations	241	242
FEM simulations	231	231
Laboratory results	248	233

Table 8.13: Comparison of stresses in lower flange with full composite action, F=150 kN

Method	G1 [MPa]	G2 [MPa]
Hand calculations	74	74
FEM simulations	64	64
Laboratory results	124	120

Table 8.14: Comparison of stresses with partial composite action, F=350 kN

Method	G1 [MPa]	G2 [MPa]
Hand calculations	-	-
FEM simulations	168	156
Laboratory results	205	207

8.3.2 Comparison between displacements

The results from the displacement calculations from the different methods are presented in the tables below. Table 8.15 and Table 8.17 exhibit results from girders subjected to a load of 350 kN. In Table 8.16 the full composite action versions of hand calculations and simulations is compared to the laboratory test, non-composite version, with the load of 150 kN. The hand calculations show a simplified version that only considers displacement of the steel beam.

Table 8.15: Comparison of displacements with non-composite action, F=350 kN

Method	G1 [mm]	G2 [mm]
Hand calculations	28,9	29,0
FEM simulations	31,9	32,6
Laboratory results	31,7	29,9

Table 8.16: Comparison of displacements with full composite action, F=150 kN

Method	G1 [mm]	G2 [mm]
Hand calculations	4,2	4,3
FEM simulations	4,6	4,7
Laboratory results	12,9	13,3

Table 8.17: Comparison of displacements with partial composite action, F=350 kN

Method	G1 [mm]	G2 [mm]
Hand calculations	-	-
FEM simulations	13,0	11,9
Laboratory results	18,1	19,9

Further to analyse the displacements from the different methods a compilation is conducted to evaluate results from each load cycle for G2 with NC action, see Figure 8.3.

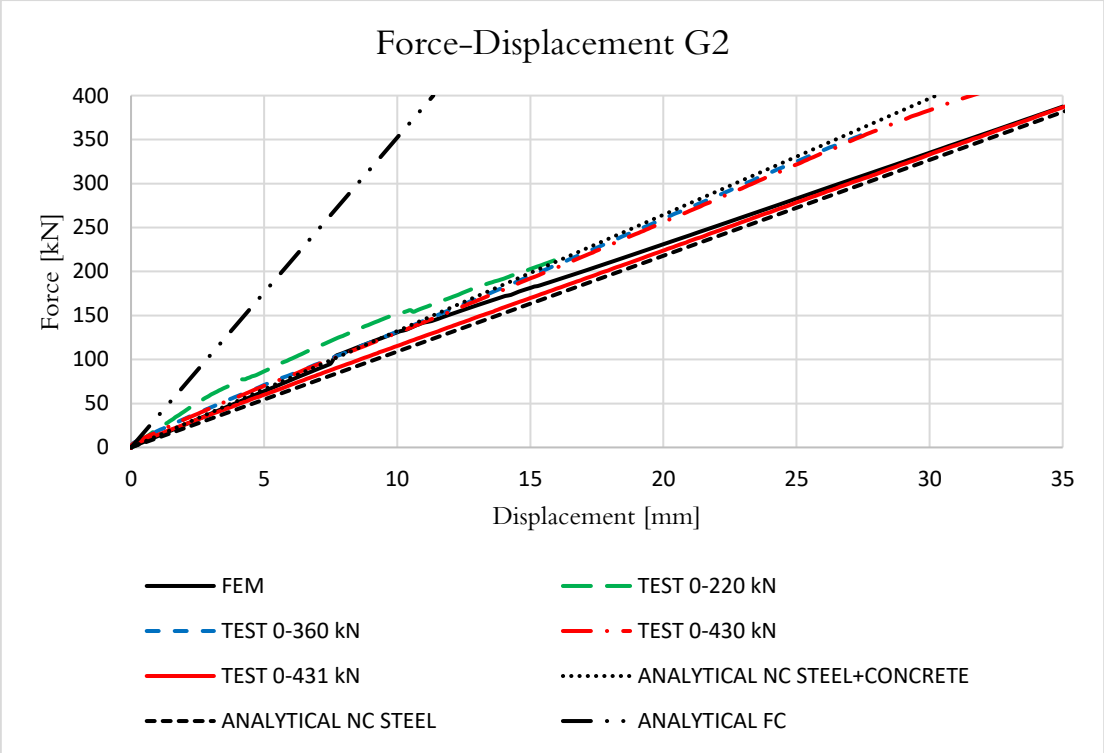

Figure 8.3: Displacements G2 with NC

8.3.3 Comparison between slips

Data for the slip between concrete and steel is presented in Table 8.18 and Table 8.19.

Table 8.18: Comparison of slips with non-composite action, F=350 kN

Method	G1 [mm]		G2 [mm]	
	A	B	A	B
FEM simulations	3,5	3,5	3,5	3,5
Laboratory results	1,9	3,3	3,5	0,0

Table 8.19: Comparison of slips with partial composite action, F=350 kN

Method	G1 [mm]		G2 [mm]	
	A	B	A	B
FEM simulations	0,1	0,1	0,1	0,1
Laboratory results	0,8	0,9	1,1	0,9

8.4 The number of coiled spring pins impact on the composite action

To analyse the impact of the number of CSPs, a varied number of connectors are tested for the partial composite action models. The models are tested for 24 CSPs to 0, with steps of four at a time. For each step, the connectors located most centrally are removed and it is done in symmetry, so equal number of connectors is removed from each side of the girder. Results is conducted for the CSPs impact on stresses and displacements, it is presented in Figure 8.4 - Figure 8.7.

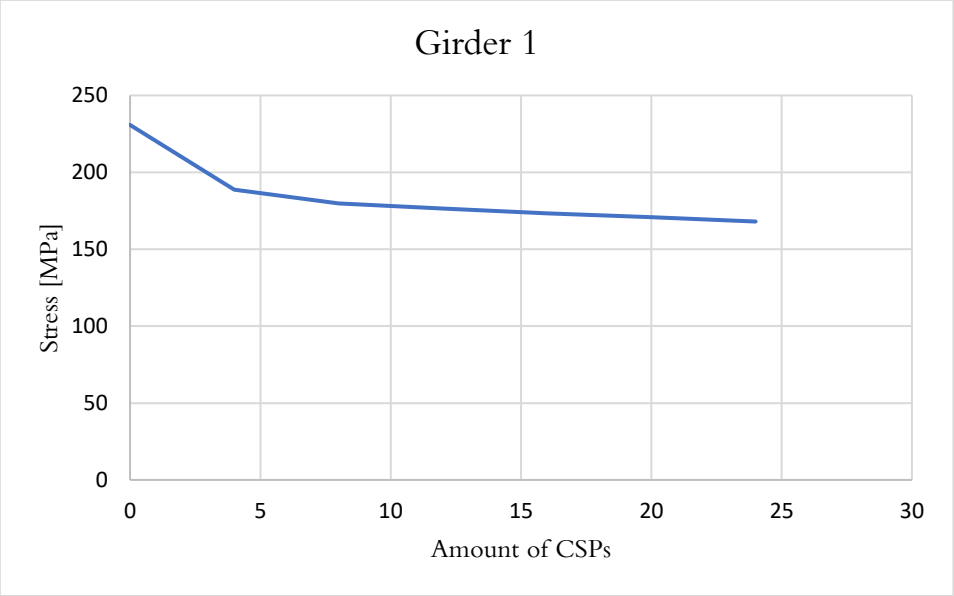

Figure 8.4: The number of CSPs impact on stress

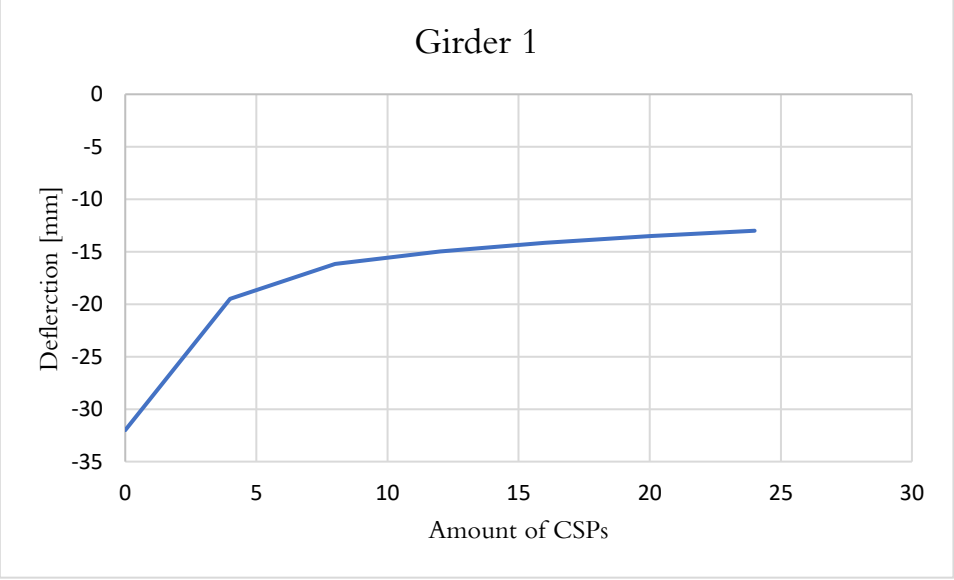

Figure 8.5: The number of CSPs impact on displacement

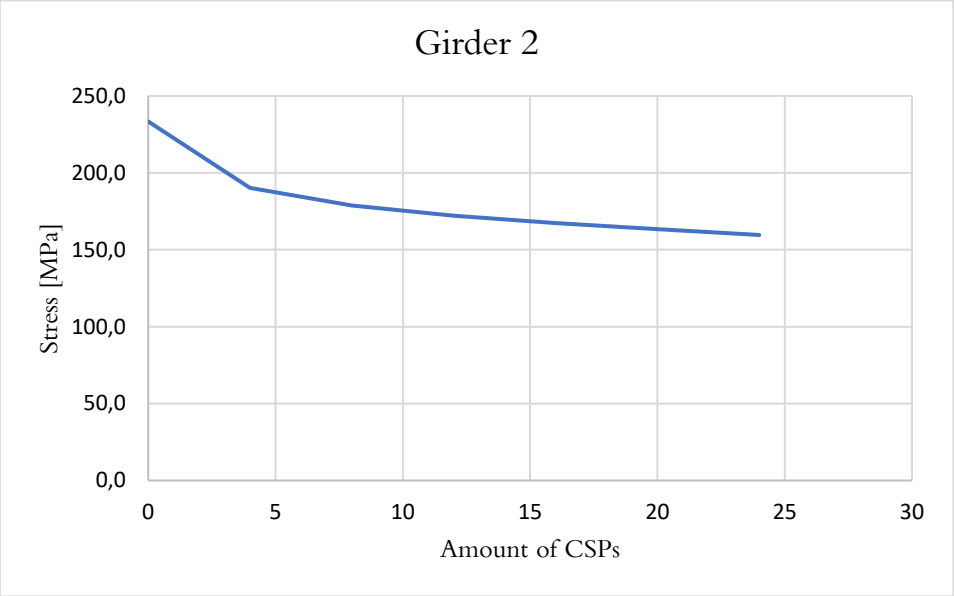

Figure 8.6: The number of CSPs impact on stress

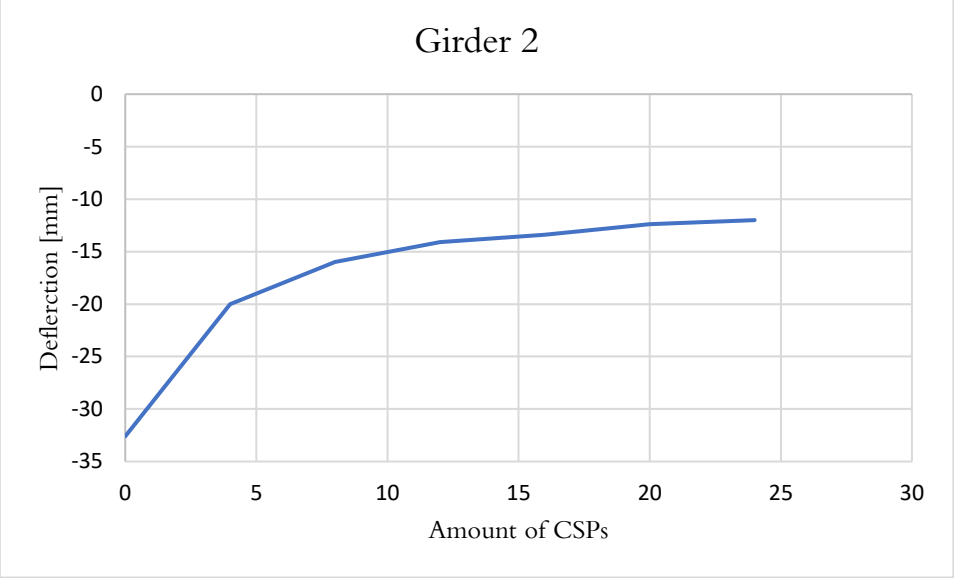

Figure 8.7: The number of CSPs impact on displacement

8.5 Impact of placement of coiled spring pins

For Girder 1, a compilation is made to analyse the impact of the placement of CSPs. The CSPs are removed from edges compared to the approach described in chapter 8.4, the results are presented in Table 8.20. An additional test is conducted to evaluate the impact of the CSPs placement. The tested beams, Girder 1 and Girder 2, is compared to a simulated version with evenly distributed pars of CSPs along the beam. The new simulated beam, called Girder 3, contains the same amount of CSPs as the simulations for Girder 1 and Girder 2. The results are presented in Table 8.20.

Table 8.20: Influence of removed CSPs, F=350 kN

CSPs	CSPs removed from centrum [MPa]	CSPs removed from edge [MPa]	CSPs with central placement [MPa]
24	168	168	154
20	171	169	154
16	173	169	156
12	176	170	160
8	180	175	169
4	189	188	185
0	231	231	231

8.6 Force – displacement relation for high load

The FEM versions of Girder 1 and Girder 2 were simulated for high loads to be comparable with the laboratory tests subjected to a load of 870 kN. The results are presented in Figure 8.8 and Figure 8.9 below.

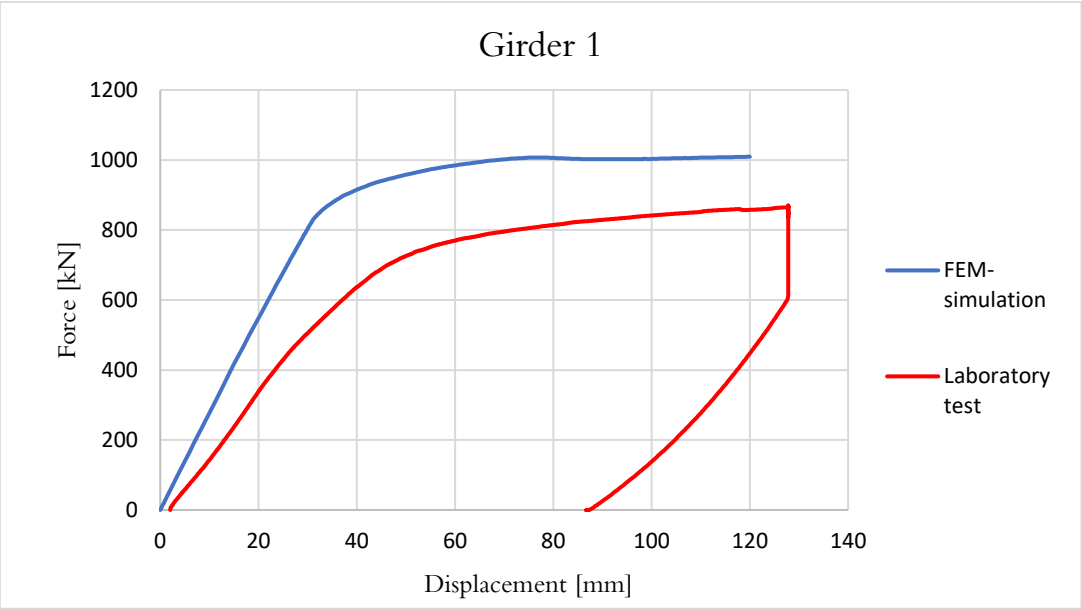

Figure 8.8: Girder 1 subjected to high load

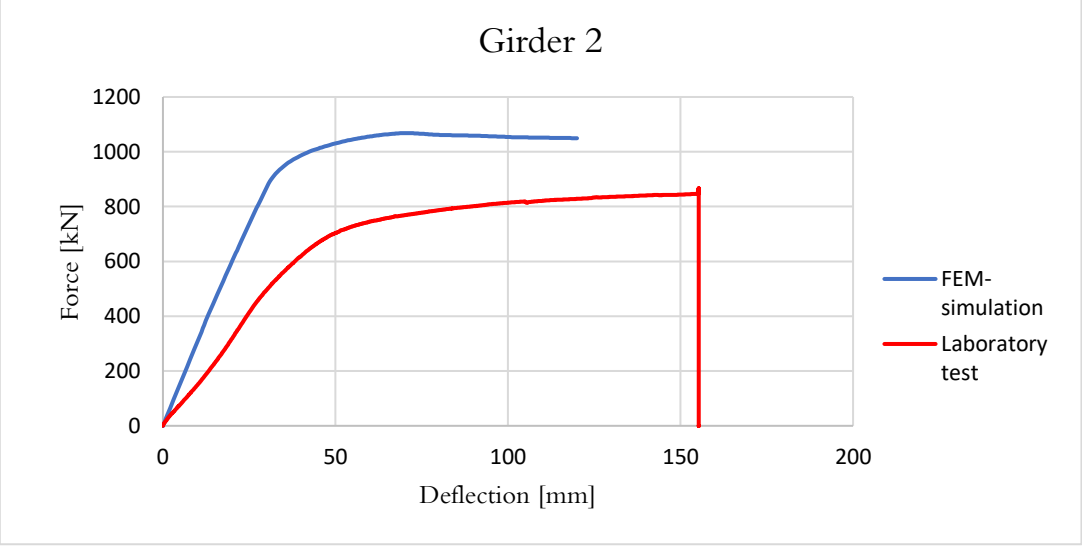

Figure 8.9: Girder 2 subjected to high load

9 Analysis and discussion

9.1 Behaviour of a girder strengthened with coiled spring pins

The general behaviour of the strengthened girders in this work, agrees with conclusions established by Stahlin (2019). In his report, a clear relationship between the CSPs and the strength of the girder were presented. This is verified by the previous laboratory tests and FEM simulations created in this thesis, thus both presents stresses 30-80 MPa lower for a load of 350 kN. This behaviour reflects on the displacement too, as the displacement is reduced with 10-20 mm between the non-composite action models to the partial composite action models. Furthermore, the relationship between the amount of CSPs and the girder strengthening, is also similar to the results presented in Stahlin (2019). For the simulated models, the first connectors have the biggest impact on the degree of composite action. Then for each CSP added the impact on the degree of composite action decreases, as it reaches closer to full composite action. Therefore, by only post-installing a few CSPs on an existing bridge, the strength can reach a significant difference.

In the laboratory tests, two girders were tested with different positions of the CSPs, Girder 1 and 2. This was conducted to evaluate whether the location of the CSPs would impact the strengthening for the girders. Except for the different CSPs positions, the only theoretical inequality, was that the concrete for Girder 1 exhibited a higher modulus of elasticity and a higher ultimate limit state, see Table 3.2. The results from the laboratory test and the FEM simulations were inconsistent, thus the simulations achieved higher stresses for Girder 1, in contrast to the tests higher stresses for Girder 2. For the simulations Girder 2 achieved 15 MPa less than Girder 1 in the lower flange, although the concrete of Girder 2 has a lower strength. This can be explained by the more evenly distributed shear connectors acting on Girder 2, thus a constant shear flow is expected to be favourable.

A new minor test was conducted to further analyse if the strength benefits observed from Girder 2 occurred from the more evenly distributed shear flow, or because the connectors are centrally positioned. The results are detailed in Table 8.20. For the CSPs removed from the centre, the stress in the lower flange increases up to 6 MPa more than the case with removed CSPs from the edge. This exhibits tendencies that more central placed connectors can be advantageous for the maximum stress in the lower flange.

To test the theory that a constant shear flow across the beam would be the most favourable case, a new test is performed, and the results are detailed in Table 8.20. A girder with new CSPs placement is created, called Girder 3. The new simulated girder contains CSPs placed with evenly distributed pairs over the entire beam, in contrast to Girder 1 and 2, which has a greater proportion placed towards the edges. Girder 3 exhibited the lowest stress of the three girders, however the difference between Girder 2 and 3 only reached 1 MPa. The laboratory test, however, had no indications on the tendencies from the simulations, as Girder 2 reached a higher stress as expected due to the lower concrete strength.

9.2 Critical factors and sources of errors in the Abaqus simulations

The FEM simulations presented in this work had the aim to replicate the behaviours by an actual girder. As the laboratory tests and the FEM simulations exhibited large differences, the critical factors and errors of the simulation are of great importance. These factors are evaluated to determine where the deviations occur and if these factors can be the total difference between simulations and the laboratory tests.

9.2.1 Impact of the friction coefficient

The friction coefficient is one of the identified factors that could possibly affect the results, thus the used coefficient is approximate, and no tests were conducted. However, by varying the friction in the non-composite models, between a large span, the stresses changed with 2,4 MPa. This difference between the extreme cases resulted only in a change of 1-2 %, so for this kind of calculation it has no significant impact.

The second test regarding the impact of the friction coefficient, evaluated the influence of different stiffnesses. For a stiff concrete, the displacement of the concrete deck may deviate from the displacement of the steel beam, thus creating gaps between the layers. These gaps would decrease the contact area between the two surfaces and could result in a reduced effect of the friction between the surfaces. In the test presented in Table 6.2, the ratio between the stresses with small and large friction coefficients resulted in a difference of around 1% regardless of stiffness. This means that no clear relationship between the stiffness and friction can be observed from the conducted test. The test is however only created for elastic material properties, with addition of full plastic input the results could be different.

The arch effect that occurred for the non-composite action models were expected to influence the impact of the friction coefficient, thus the contact surface gets decreased with gaps between steel beam and concrete deck. The final non-composite action test for the friction coefficient was therefore created to evaluate the arch effects impact on the friction behaviour of the girder. For the girder presented in Figure 6.2, no visible gaps appeared between steel and concrete, this in contrast to the ordinary non-composite version presented in Figure 8.1. As the ordinary case has two large gaps between the materials, the contact surface is decreased, with a smaller surface for the friction to act on. The comparison presented in Table 6.3 indicates that the arch effect has an impact on the sensitivity of the friction coefficient, thus the ratio between the stresses increased from 1-3,5% and the displacement from 1-5%.

The conducted tests indicates that the input of friction coefficient has no significant impact on the non-composite girders tested in this case. However, there is always a small impact of the coefficients and for accurate simulations a friction test is preferable, otherwise a deviation up to 1% can be expected. The arch effect is considered to have an impact of the coefficient, as the tests with a load that counteracted this effect exhibited a greater impact from the coefficient.

For partial composite action, presented in Table 6.4, the differences were small even though the girders acting together with no arch effects. The expected reason for this is the already high degree of composite action, illustrated in Figure 8.1 and Figure 8.6. The first installed CSPs affect the strength significantly, then for each connector added the impact gets smaller. As the friction acting together with the CSPs the same behaviour is expected, meaning that the friction coefficient has a small impact with a high degree of composite action.

9.2.2 Impact of viscosity parameter

As observed in Table 6.4, there was minimal impact on the variation in stress when changing the viscosity parameter from 0,0005 to 0,01, while significantly reducing the simulation time. Leveraging this, the authors conducted numerous simulations, testing the impact of other parameters and adjusted the model within a shorter time frame, streamlining the modelling process. Subsequently, upon achieving satisfactory results, we conducted final simulations using a lower viscosity value to ensure the most accurate results.

9.2.3 Impact of dilation angle

As emphasized in chapter 6.3 the dilation angle is described, by several sources, to have a major impact of the simulation results. However, as seen in Table 6.5, the results of the sensitivity analysis tell a different story. The dilation angle is set to five different values ranging from 10–50 degrees, but the resulting stresses only varies approximately 1 MPa, which is almost negligible. An explanation to this may be the failure mode of the beam. The failure mode is caused by bending and not shearing where the impact of the dilation angle probably would be greater.

9.2.4 Sources of error in Abaqus simulations

Throughout the creation of the FEM models, simplifications have been made to decrease the run time for the simulations. In addition to these simplifications, some required input data has not been available, as it would have required new laboratory tests. The potential sources of errors that have not been further studied is presented below.

- All stress – strain input for both steel and concrete are based on provided maximum values. This means that the complete stress - strain curve is created from approximate calculation models from the maximum yield stress and ultimate limit state.
- No material tests have been conducted on the reinforcement bars; actual values may deviate. The value for the ultimate limit state is roughly estimated from literature.
- The choice of the plasticity factors is conducted in accordance with literature, without further studies about the differences between this case and the literature.
- The supports are defined as boundary conditions along lines traversing the steel beam, rather than being modelled as actual roller supports. This means that the characteristics of the movement between support and steel beam are not considered in the model.
- The CSPs were not modelled as parts and were only defined as non-linear connectors using the test-data from the push-out tests from Hällmark et al., (2021). Consequently, no holes were modelled in either the concrete or the steel. The connector ends were placed at the bottom of the upper flange and the bottom of the concrete deck, leading to an inaccurate portrayal of their actual length.
- The two welded headed studs used in the laboratory test were not created in the FEM models.

9.3 Comparison between laboratory tests, FEM simulations and hand calculations

For the stresses presented and analysed below, only the stress below the point load, in the lower flange is considered. The displacement always refers to the girder's maximum values.

9.3.1 Non-composite action

The stress comparison in the lower flange shows variations that lie within a reasonable range of 0-20 MPa. The minor deviations could stem from the uncertain factors in the FEM simulations. These factors include the friction coefficient between the steel and concrete interface, as well as the dilation angle and viscosity parameter used to describe the concrete behaviour during deformation.

Another possible reason for the deviation is the variation in measurement points between the laboratory tests and the simulations. In the laboratory tests the stress was measured at a specific point, while in the simulations the stress was measured across an area, as shown in the figure below.

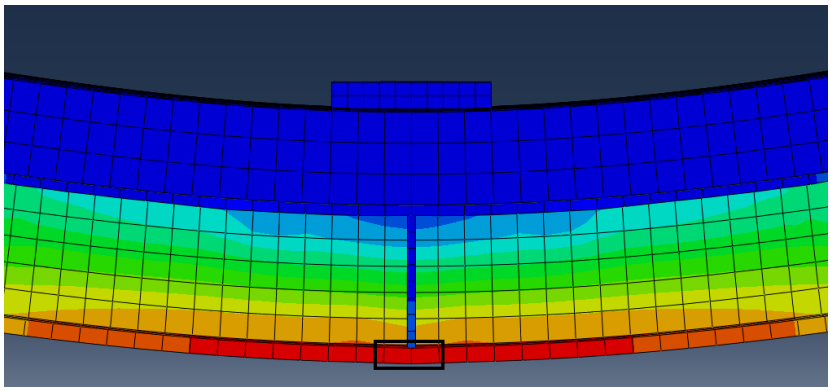

Figure 9.1: Measuring location for stresses

The result for the displacements exhibits low differences as the values varies between 0-3 mm between all methods for the load of 350 kN. By comparing the results from the load cycles for Girder 2, further analysis of the behaviour of the FEM model can be conducted. Initially, the FEM model behaves similar to the analytical version with acting steel and concrete, see the figure below. The displacement in the FEM simulations is linear to the compared test results (the blue dotted line in the figure below) up to 80 kN. From the load of 80 kN, plastic strains in the concrete begins to accumulate, see Figure 8.2. After the strain increases, the slope of the line is changing direction from results close to analytical, with both steel and concrete, to the version with only acting steel. The same behaviour occurs for the laboratory test, but first at the second last load cycle at a load of 350 kN. For the last load cycle of the NC models, the displacement is almost identical to the values from the FEM model, after higher loads are achieved. This means that the main difference between the models is for which load plastic strain occurs, as the concrete in the FEM version reaches it before. Further, would the displacement values almost be identical between the methods if the results were retrieved from a later load cycle.

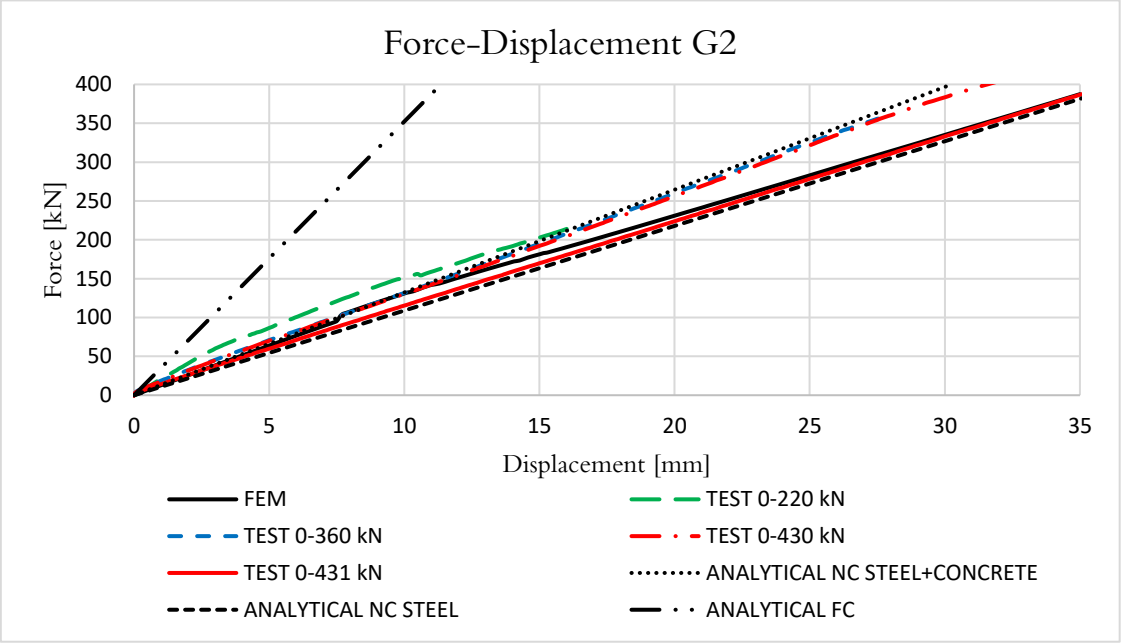

Figure 8.3: Displacements G2 with NC

By comparing the slip data for the non-composite version, the relationship between the slip and the displacement acts as expected. For the first load cycle up to 350 kN, the laboratory test for both girders exhibited lower slip than the FEM simulations, this is also reflected in the results for the displacements. The laboratory test with lower slip has also lower displacement compared to the FEM versions. This ratio is expected, as the slip between the members has a big influence for the ratio of composite action in a girder, as described in chapter 2. Therefore, beams with small slip should have lower displacement as a higher degree of composite action is obtained. The impact can also be exhibited by comparing Girder 1 and 2 for the laboratory tests. G2 displays the lowest values in both slip and displacement when compared to G1, which demonstrates higher values for both parameters. This means that a larger displacement is achieved on G1, even though the girder has stronger concrete properties.

The stress results can also be analysed by comparing it with the results in slip. The deviation for the stresses is most extensive for G1, for G2 the stresses between the laboratory and simulations are almost identical. The expected explanation for this is the different slip in the laboratory tests. For G1 is the slip between simulations and laboratory tests similar, however resulting in the biggest deviation. G2 in contrast, exhibits differences in the slip, still the results for the stresses between the laboratory and the simulations is almost identical. This suggests that if the simulations had the same slip as the laboratory tests, the FEM simulations would exhibit lower stress.

In summary, the outcomes in terms of stress, displacement and slip are reasonable for non-composite action. The most significant difference between the models is for which load plastic strain occurs in the concrete. For the last load cycle with a load of 350 kN the results are almost identical between FEM simulations and the laboratory tests.

9.3.2 Full composite action

The results for full composite action are not of primary focus, as no specific laboratory test were conducted. The data is analysed for the laboratory test values of the non-composite action beams subjected to a load of 150 kN. The lower load is used to replicate the behaviour of full composite action in the laboratory test; thus, the slips is still small and expected to behave close to a full composite action version.

The stresses for FC presented in Table 8.13 exhibits values more deviant than the results for the NC action models, as the difference between laboratory results and the other methods, reaches 50-60 MPa. An increased difference can however be expected, as the replicated version of FC action contains small slips in contrast to the calculated and simulated versions. To improve these results, even smaller loads would have been beneficial to test, since plastic strain in the concrete tension zone occurred already at 80 kN for the FEM models.

The difference between the hand calculations and the FEM simulations seems to be consistent, thus the hand calculations reached 10-20 MPa more stress in the lower flange for both the NC and the FC versions. However, these differences can be considered within a reasonable range as the calculations are based on simple beam theory. In addition, could the different measurement points impact, as the hand calculations presents stress in the middle of the flange instead of the edge.

The displacement in the replicated full composite version from the laboratory tests, exhibits significantly greater values than the displacements from simulations and hand calculations. For the expected case, a beam subjected to high stress, should have a displacement that replicates the stresses. Therefore, the results for displacement in the full composite version seems reasonable, thus the high stresses also result in high displacements.

9.3.3 Partial composite action

In the same way as for full composite action, the difference between the stress from the FEM simulations and the laboratory test seems high. However, the deviation in the PC models can be expected, due to the different load cycles. In the laboratory tests, the concrete reaches plastic strain in the middle below the load-cell, as seen in Figure 8.2, before CSP is added. In contrast to the laboratory tests, the CSPs in the FEM simulations are added from the beginning. This means that the concrete is strengthened from the beginning and expected to withstand higher loads before plastic strain occurs. Consequently, this would result in the concrete contributing to the load distribution for higher loads in the FEM models than the laboratory tests.

The stress displacement behaviour obtained for full composite action also applies to partial composite action. The differences between the results in stresses are also reflected in the results for the displacement, thus the FEM models achieves less displacement than the laboratory tests. This occurrence probably arises from cracks in the middle of the concrete beam, making the cross section less rigid than the FEM models, which hasn't encountered any stress levels before being strengthened with CSPs.

By comparing the slip data for partial composite action, the FEM simulations exhibits lower slip than the laboratory tests, with a difference between 0,7–1 mm. As described in chapter 2, the slip between the members has a big influence for the ratio of composite action in a girder. This is the case between the FEM simulations and the laboratory tests, where the FEM simulations has the lowest stress and the smallest slip.

Two additional simulations were conducted for partial composite action, where the girders were loaded to 870 kN, to be compared to the maximum load applied in the physical test. The FEM simulations reached a higher yield strength with a difference of approximately 100-200 kN, the greater difference occurs for Girder 2. No precise comparison can be done for the ultimate limit state since the failure load was not reached in the laboratory tests. It can be concluded that the simulated girders achieved higher loads for the same displacements compared to the physical girders, which aligns with previous analyses for PC models. Even here, it is expected to depend on the cracks from prior loading in the laboratory tests.

9.3.4 Deviations in the laboratory tests

By comparing the results from the hand calculations and FEM simulations with the laboratory tests, some deviations emerged. For the non-composite version, the concrete weakened for completely different loads, approximately at 80 kN for simulations and 350 kN for the tests. This is expected to have resulted in some differences in stress and deflection between FEM simulations and laboratory tests.

For full composite action there were more significant differences than for the non-composite version. This was displayed by the almost doubled values in stress and displacement for the FC version. The expected explanation for the differences is that the assumption of using a NC model for a load of 150 kN is not close enough to replicate a FC model.

The partial composite action model also exhibited differences between laboratory tests, simulations, and calculations, although not as large as for FC action. The differences is expected to be a result of the different load cycles in the laboratory tests that were neglected in the FEM simulations and the hand calculations

10 Conclusions and recommendations

In accordance with previous research, CSPs improve the strength of composite girders. When conducting the simulations, the first connectors have the biggest impact on the degree of composite action. The influence gets smaller as the degree of composite action approaches full composite action, and the neutral axis of the cross-section gets closer to the concrete slab.

No conclusions can be drawn whether the placement of the CSPs has an impact on the strengthening, thus the tendencies obtained from the simulations were not verified by the laboratory test. The FEM simulations indicated that CSPs evenly distributed and placed more central could improve the strengthening for similar setups.

The identified critical factors as friction coefficient, viscosity parameter and dilation angle exhibit small impact on the total strength of the girders, as long as they were chosen within a reasonable range, found in literature. To obtain a model with very high accuracy, however, these factors are important but difficult to determine.

The simulated non-composite girders replicate the results of the displacement observed during the last load cycle in the laboratory test. This implies that composite girders simulated in Abaqus can accurately replicate the behaviour of the tested girders.

The FEM simulated partial composite girders exhibited greater strength compared to their laboratory counterparts. This outcome could be derived from that the concrete for the tested girders probably had some cracks from the previous loading steps before they were strengthened.

10.1 Further research

- Make further tests whether the placement of CSPs have an impact on the total strengthening. This could be done by doing additional laboratory tests, with CSPs placed only in the centre and CSPs placed evenly distributed for instance. With this type of analysis, the general behaviour of the placement of CSPs could be determined and the differences between the methods presented in this report could be clarified.
- Do further analysis on the differences in stresses and displacements between simulations, calculations, and the laboratory tests. This can be accomplished by first reviewing the laboratory results. Since the test results are extensive, only a part of the test results has been analysed. This can be followed by adding hand calculations for partial composite action to verify the presented FEM simulations.
- To further increase the accuracy of the FEM models the simulated girders could undergo the same load cycles as the ones in the laboratory test. Alternatively, the cracks could be simulated directly in the concrete prior to loading of the strengthened girder.
- Do additional tests to evaluate if the concrete tested in the laboratory tends to reach plastic strains before the FEM simulations for composite girders.
- After the differences between the laboratory test and the other methods is clarified, it would be interesting to use the calibrations from the FEM models in a concept bridge. By doing this in a wider scale, the CSPs strengthening effect on existing bridges could be determined with FEM simulations with high precision.

11 References

Ansys. (28 April 2021). *The fundamentals of FEA meshing for structural analysis.* https://www.ansys.com/blog/fundamentals-of-fea-meshing-for-structural-analysis

Apostolopoulos, A., Matikas, T.E. (2018). *The impact of corrosion and inelastic buckling on low cycle fatigue life of steel bars.* Department of Material Science and Engineering, University of Ioannina, Greece. https://www.researchgate.net/publication/328115478_The_impact_of_corrosion_and_inelastic_buckling_on_low_cycle_fatigue_life_of_steel_bars

Autodesk. (8 October 2023). *How to perform a mesh convergence study.* https://www.autodesk.com/support/technical/article/caas/sfdcarticles/sfdcarticles/How-to-Perform-a-Mesh-Convergence-Study.html

Bilal, K.A., Mahamid, M., Amin Hariri-Ardebili, M., Tort, C & Ford, T. (2023). *Parameter Selection for Concrete Constitutive Models in Finite Element Analysis of Composite Columns.* Buildings 2023, 13, 1759. https://doi.org/10.3390/buildings13071759

Caprili, S., Salvatore, W (2018). *Mechanical performance of steel reinforcing bars in uncorroded and corroded conditions.* University of Pisa, Department of Civil and Industrial Engineering, Italy. https://www.sciencedirect.com/science/article/pii/S2352340918304256

Collin, P., Johansson, B. & Sundqvist, H. (5ed. 2012). *Steel Concrete Composite Bridges.* Luleå University of Technology (LTU) Division of Structural Engineering.

Dassault Systèmes. (7 November 2014). *Abaqus Analysis User's Guide.* Providence, RI, USA: http://130.149.89.49:2080/v6.14/books/usb/default.htm

Demir, A., Ozturk, H., Edip, K., Stojmanovska, M & Bogdanovic, A. (2018). *Effect of vicosity parameter on the numerical simulation of reinforced concrete deep beam behavior.* Faculty of Engineering, Department of Civil Enginering, Sakarya University, Sakarya, Turkey Institute of Earthquake Engineering and Engineering Seismology, Ss. Cyril and Methodius University, Skopje, Macedonia. https://www.tojsat.net/journals/tojsat/articles/v08i03/v08i03-09.pdf

El Sarraf, R., Iles, D., Momtahan, A., Easey, D., & Hicks, S. (2013). *Steel-concrete composite bridge design guide.* NZ Transport Agency. https://www.researchgate.net/publication/258511447_Steel-concrete_composite_bridge_design_guide

Guo, Q., Chen, Q., Xing, Y., Xu, Y., & Zhu, Y. (2020). *Experimental study of friction resistance between steel and concrete in prefabricated composite beam with high-strength frictional bolt.* Advances in Materials Science and Engineering, vol. 2020, Article ID 1292513, 13 pages. https://doi.org/10.1155/2020/1292513.

Hällmark, R., Nilforoush, R., Vestman, V., & Colin, P. (2021). *Testing of composite girders with coiled spring pin shear connectors.* Luleå University of Technology (LTU) Department of Civil, Environmental and Natural Resources Engineering. *https://vpp.sbuf.se/Public/Documents/ProjectDocuments/838c40ec-8511-49a6-a995-a99547e463e4/FinalReport/SBUF%2013227%20-%20Beam%20tests_Final_Artikel.pdf*

Hällmark, R., Collin, P., & Hicks, S (2019). *Post-installed shear connectors: Push-out tests of coiled spring pins vs. headed studs.* Luleå University of Technology (LTU) Department of Civil, Environmental and Natural Resources Engineering. https://www.sciencedirect.com/science/article/pii/S0143974X18309064

Hällmark, R., (2018). *Composite Bridges, Innovative ways of achieving composite action.* Doctoral thesis, Luleå University of Technology (LTU) Department of Civil, Environmental and Natural Resources Engineering. https://www.diva-portal.org/smash/record.jsf?pid=diva2%3A1249244&dswid=1909

Hällmark, R., Vestman, V., Collin, P., & Amani, M. (n.d.). *Framtagande av dimensioneringsriktlinjer för förstärkning av stålbalksbroar via skapande av partiell samverkan.* Luleå University of Technology (LTU) Department of Civil, Environmental and Natural Resources Engineering.

Isaksson, T & Mårtensson, A. (2019). *Byggkonstruktion, Regel- och formelsamling.* (4 edition) Studentlitteratur AB.

Jabbar, M. A. (2023). *Impact of Failure-surface Parameters of Concrete Damage Plasticity Model on the Behavior of Reinforced Ultra-high Performance Concrete Beams.* https://www.researchgate.net/publication/368661782_Impact_of_Failure-surface_Parameters_of_Concrete_Damage_Plasticity_Model_on_the_Behavior_of_Reinforced_Ultra-high_Performance_Concrete_Beams.

Jankowiak, T., & Lodygoski, T (2005). *Identification of parameters of concrete damage plasticity constitutive model.* Poznan University of Technology, Institute of Structural Engineering (ISE). https://www.researchgate.net/profile/Tomasz-Jankowiak/publication/228525599_Identification_of_parameters_of_concrete_damage_plasticity_constitutive_model/links/0c960519d19470dbb8000000/Identification-of-parameters-of-concrete-damage-plasticity-constitutive-model.pdf

Kwon, G. (2008). *Strengthening Existing Steel Bridge Girders by the Use of Post-Installed Shear Connectors.* Doctoral thesis, The University of Texas at Austin. https://library.ctr.utexas.edu/ctr-publications/0-4124-1.pdf

Nayal, R., & Rasheed, H. A. (2006). *Tension Stiffening Model for Concrete Beams Reinforced with Steel and FRP Bars. Journal of Materials in Civil Engineering,* 18(6). https://www.researchgate.net/publication/245308166_Tension_Stiffening_Model_for_Concrete_Beams_Reinforced_with_Steel_and_FRP_Bars

Norlin, B. (n.d.). *Lecture 12 Composite beams with partial composite action.*

Olsson, D. (2017). *Achieving Composite Action in Existing Bridges.* Master's thesis, Luleå University of Technology (LTU) Department of Civil, Environmental and Natural Resources Engineering. https://ltu.diva-portal.org/smash/record.jsf?dswid=-1625&pid=diva2%3A1066328&c=1&searchType=SIMPLE&language=sv&query=david+olsson+Achieving+Composite+Action+in+Existing+Bridges&af=%5B%5D&aq=%5B%5B%5D%5D&aq2=%5B%5B%5D%5D&aqe=%5B%5D&noOfRows=50&sortOrder=author_sort_asc&sortOrder2=title_sort_asc&onlyFullText=false&sf=all

Schoening, J., Hegger, J. (2015). *Concrete elements reinforced with large diameters – bons behaviour and lapped joints.* Institute of Structural Concrete, RWTH Aachen University, Germany. https://www.researchgate.net/publication/305790312_CONCRETE_ELEMENTS_REINFORCED_WITH_LARGE_DIAMETERS_-_BOND_BEHAVIOUR_AND_LAPPED_JOINTS

Spirol. (2022). *Coiled Spring Pins*. https://www.spirol.com/assets/files/cldp-coiled-spring-pins-design-guide-us.pdf

SS-EN 1992-1-1. (2005). *Eurocode 2: Design of concrete structures – part 1-1: General rules and rules for buildings*. Brussels, CEN – European Committee for standardization. https://www.sis.se/en/produkter/construction-materials-and-building/construction-industry/technical-aspects/ssen1992112005a120142/

SS-EN 1993-1-1. (2005). *Eurocode 3: Design of steel structures - Part 1-1: General rules and rules for buildings.* Brussels, CEN – European Committee for standardization. https://www.sis.se/en/produkter/construction-materials-and-building/construction-industry/technical-aspects/ssen1993112005/

SS-EN 1993-2. (2017). *Eurocode 3: Design of steel structures – Part 2: Steel bridges*. Brussels, CEN – European Committee for standardization. https://www.sis.se/en/produkter/construction-materials-and-building/construction-industry/technical-aspects/ssen199322006/

SS-EN 1994-1-1. (2004). *Eurocode 4: Design of composite steel and concrete structures – Part 1-1: General rules and rules for buildings.* Brussels, CEN – European Committee for standardization. https://www.sis.se/produkter/byggnadsmaterial-och-byggnader/byggnadsindustrin/tekniska-aspekter/ssen1994112005ac2009/

SS-EN 1994-2. (2005). *Eurocode 4: Design of composite steel and concrete structures – part 2: General rules and rules for bridges*. Brussels, CEN – European Committee for standardization. https://www.sis.se/produkter/byggnadsmaterial-och-byggnader/byggnadsindustrin/tekniska-aspekter/ssen199422005/

Stahlin, S. (2019). *Non-Linear FE-Analysis of a Composite Action Girder with Coild Spring Pins as Shear Connectors*. Master's thesis, Luleå University of Technology (LTU) Department of Civil, Environmental and Natural Resources Engineering. https://ltu.diva-portal.org/smash/record.jsf?pid=diva2%3A1317473&dswid=9121

Tjernberg, J. (2022). *Strengthening of non-composite bridges byt Partial Composite Action*. Master's thesis, Luleå University of Technology (LTU) Department of Civil, Environmental and Natural Resources Engineering. https://ltu.diva-portal.org/smash/record.jsf?pid=diva2%3A1640776&dswid=9082

Vestman, V. (2023). *I-girder Composite Bridges with Lateral Bracing*. Licentiate thesis, Luleå University of Technology (LTU) Department of Civil, Environmental and Natural Resources Engineering. https://www.diva-portal.org/smash/record.jsf?pid=diva2%3A1745142&dswid=-605

Wahalathantri, B.L., Thambiratnam, D.P., Chan, T.H.T., & Fawzia, S. (2011). *A material model for flexural crack simulation in reinforced concrete elements using ABAQUS*. In

Proceedings of the First International Conference on Engineering, Designing and Developing the Built Environment for Sustainable Wellbeing, Queensland University of Technology, Brisbane, Qld, pp. 260-264. https://www.researchgate.net/publication/277988115_A_Material_Model_for_Flexural_Crack_Simulation_in_Reinforced_Concrete_Elements_Using_ABAQUS

Yun, X., Gardner, L. (2017). *Stress-strain curves for hot-rolled steels*. Journal of Constructional Steel Research. https://www.researchgate.net/publication/317286690_Stress-strain_curves_for_hot-rolled_steels

Appendix

11.1 Appendix A – Construction documents for steel beam and concrete deck

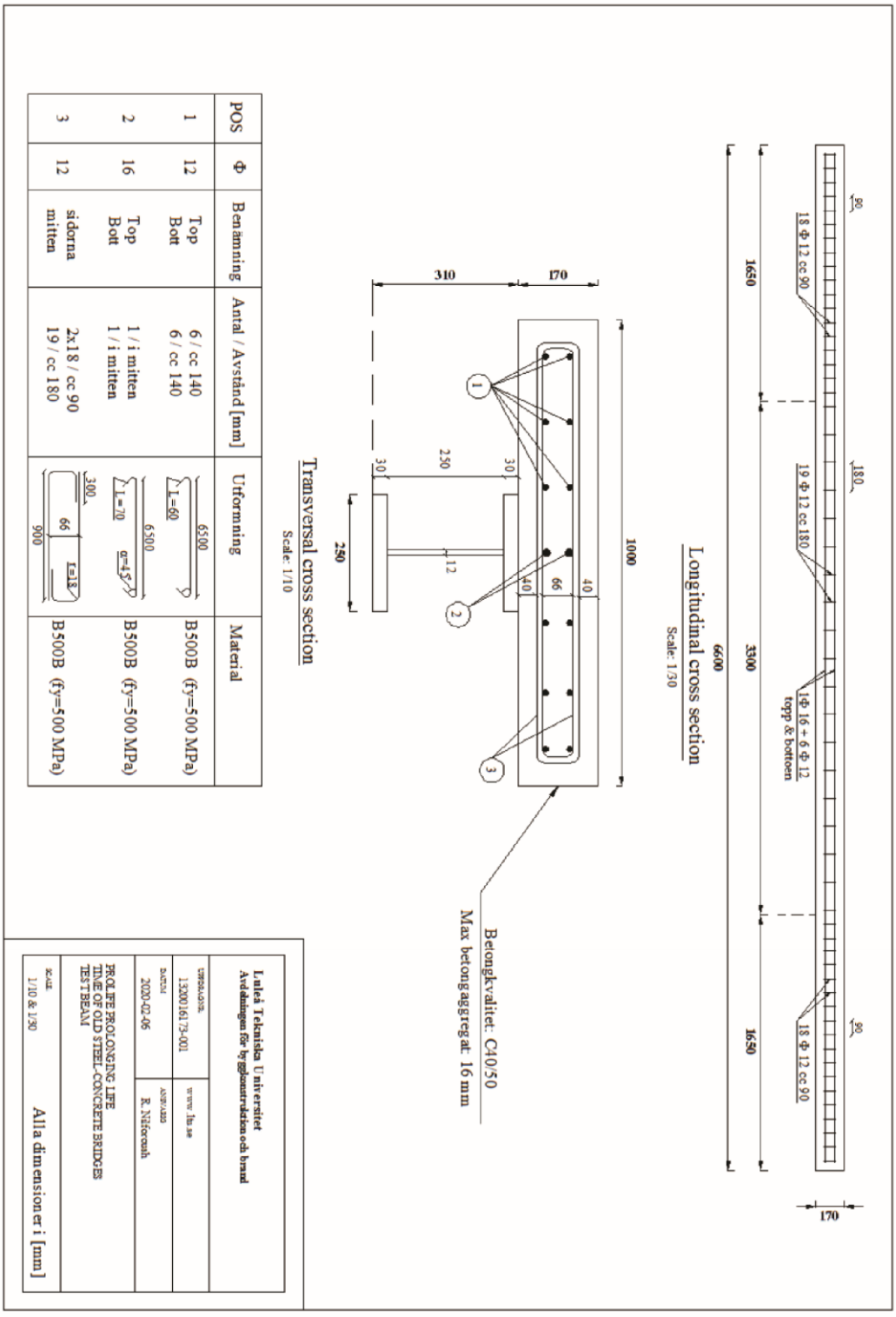

POS	Φ	Benämning	Antal / Avstånd [mm]	Utformning	Material
1	12	Top Bott	6 / cc 140 6 / cc 140	6500 L=60	B500B (fy=500 MPa)
2	16	Top Bott	1 / i mitten 1 / i mitten	6500 L=70 α=45°	B500B (fy=500 MPa)
3	12	sidorna mitten	2x18 / cc 90 19 / cc 180	300 66 t=18 900	B500B (fy=500 MPa)

Figure A.1: Reinforcement details of the concrete slabs

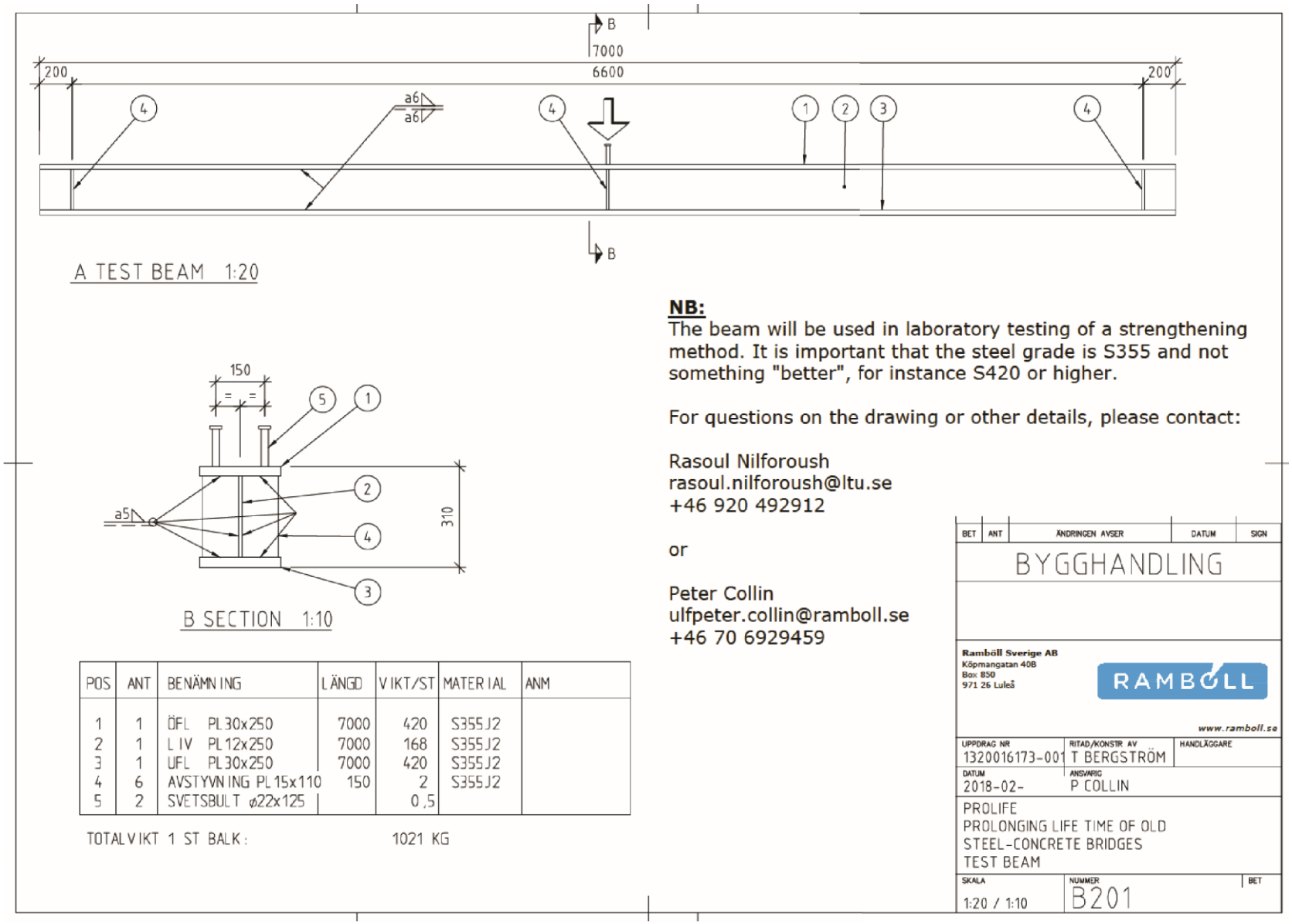

POS	ANT	BENÄMNING	LÄNGD	VIKT/ST	MATERIAL	ANM
1	1	ÖFL PL30x250	7000	420	S355J2	
2	1	LIV PL12x250	7000	168	S355J2	
3	1	UFL PL30x250	7000	420	S355J2	
4	6	AVSTYVNING PL15x110	150	2	S355J2	
5	2	SVETSBULT ø22x125		0,5		

TOTALVIKT 1 ST BALK: 1021 KG

Figure A.2: Details of steel girder

11.2 Appendix B – Stress and strain values for steel and concrete

Table B.1: Material input for the steel parts

Web		Flange		Reinforcement	
σ_c [Mpa]	ε_c [-]	σ_c [Mpa]	ε_c [-]	σ_c [Mpa]	ε_c [-]
0	0	0	0	0	0
447	0,002	407	0,002	500	0,002
447	0,022	407	0,020	500	0,023
447	0,022	407	0,020	500	0,023
458	0,026	417	0,024	512	0,027
469	0,030	427	0,028	525	0,031
480	0,034	437	0,032	537	0,035
491	0,038	447	0,036	550	0,039
502	0,042	457	0,040	561	0,043
512	0,046	466	0,044	572	0,047
521	0,050	475	0,048	582	0,051
528	0,054	483	0,052	589	0,055
534	0,058	490	0,056	595	0,059
539	0,062	495	0,060	600	0,063
543	0,066	500	0,064	603	0,067
546	0,070	503	0,068	607	0,071
549	0,074	506	0,072	609	0,075
551	0,078	509	0,076	612	0,079
553	0,082	511	0,080	614	0,083
555	0,086	513	0,084	617	0,087
557	0,090	515	0,088	619	0,091
559	0,094	517	0,092	639	0,131
561	0,098	519	0,096	-	-
563	0,102	521	0,100	-	-
565	0,106	523	0,104	-	-
567	0,110	524	0,108	-	-
569	0,114	526	0,112	-	-
571	0,118	528	0,116	-	-
573	0,122	529	0,120	-	-
575	0,126	531	0,124	-	-
576	0,130	533	0,128	-	-
578	0,134	535	0,132	-	-
579	0,137	536	0,136	-	-
-	-	538	0,140	-	-
-	-	540	0,144	-	-
-	-	541	0,148	-	-
-	-	541	0,149	-	-

Table B.2 presents a rough estimation for ultimate stress for reinforcement of type K500B, this is necessary to produce the approximate stresses in Table B.1. The mean value calculated in the table are based on combined test values from the reports Caprili, S & Salvatore, W (2018), Schoening, J & Hegger, J (2015) & Apostolopoulos, A & Matikas, T.E. (2018)

Table B.2: Approximate ultimate stress for reinforcement of type K500B

B500B	1 [MPa]	2 [MPa]	3 [MPa]	4 [MPa]
θ_{10}	637	-	-	-
θ_{12}	627	621	-	-
θ_{16}	616	668	671	635
Mean value: 639 MPa				

Table B.3: Concrete material values in tension for Girder 1

σ_t [MPa]	ε_t [-]	d_t [-]	$\varepsilon_{0t,el}$ [-]	$\varepsilon_{t,ck}$ [-]	$\varepsilon_{t,el}$ [-]	$\varepsilon_{t,pl}$ [-]
4,4	0,0001	0	0,000128	0	0,000128	0
3,388	0,0002	0,23	9,88E-05	6,16E-05	0,000128	3,21E-05
1,98	0,0005	0,55	5,77E-05	0,000455	0,000128	0,00038
0,44	0,0011	0,9	1,28E-05	0,001103	0,000128	0,00099

Table B.4: Concrete material values in compression for Girder 1

σ_c [MPa]	ε_c [-]	d_c [-]	$\varepsilon_{0c,el}$ [-]	$\varepsilon_{c,in}$ [-]	$\varepsilon_{c,el}$ [-]	$\varepsilon_{c,pl}$ [-]
0	0	0	0	0	0	0
3,570	0,0001	0	0,000104	-4E-06	0,000104	-4E-06
7,070	0,0002	0	0,000206	-6,1E-06	0,000206	-6,1E-06
13,85	0,0004	0	0,000404	-3,6E-06	0,000404	-3,6E-06
20,30	0,0006	0	0,000592	8,18E-06	0,000592	8,18E-06
26,39	0,0008	0	0,000769	3,05E-05	0,000769	3,05E-05
32,08	0,0010	0	0,000935	6,47E-05	0,000935	6,47E-05
37,32	0,0012	0	0,001088	0,00011	0,001088	0,00011
42,03	0,0014	0	0,001225	0,00018	0,001225	0,00018
46,16	0,0016	0	0,001346	0,00025	0,001346	0,00025
49,61	0,0018	0	0,001446	0,00035	0,001446	0,00035
52,29	0,0020	0	0,001525	0,00048	0,001525	0,00048
54,70	0,0025	0	0,001590	0,00091	0,001595	0,00091
54,80	0,0024	0	0,001598	0,00082	0,001598	0,00082
48,47	0,0030	0,115	0,001413	0,00159	0,001598	0,00140
28,28	0,0035	0,484	0,000825	0,00268	0,001598	0,00190

Table B.5: Concrete material values in tension for Girder 2

σ_t [MPa]	ε_t [-]	d_t [-]	$\varepsilon_{0t,el}$ [-]	$\varepsilon_{t,ck}$ [-]	$\varepsilon_{t,el}$ [-]	$\varepsilon_{t,pl}$ [-]
4,3	0,0001	0,00	0,000128	0	0,000125	0
3,311	0,0002	0,25	9,85E-05	6,14E-05	0,00012828	2,90E-05
1,935	0,0005	0,56	5,75E-05	0,000454	0,00012828	0,000381
0,43	0,0011	0,90	1,27E-05	0,001101	0,00012828	0,000982

Table B.6: Concrete material values in compression for Girder 2

σ_c [MPa]	ε_c [-]	d_c [-]	$\varepsilon_{0c,el}$ [-]	$\varepsilon_{c,in}$ [-]	$\varepsilon_{c,el}$ [-]	$\varepsilon_{c,pl}$ [-]
0	0	0	0	0	0	0
3,49	0,0001	0	0,000102	-1,79E-06	0,00010	-1,8E-06
6,91	0,0002	0	0,000201	-1,39E-06	0,00020	-1,4E-06
13,50	0,0004	0	0,000394	6,45E-06	0,00039	6,4E-06
19,74	0,0006	0	0,000576	2,45E-05	0,00058	2,4E-05
25,60	0,0008	0	0,000746	5,38E-05	0,00075	5,4E-05
31,02	0,0010	0	0,000904	9,56E-05	0,00090	9,6E-05
35,96	0,0012	0	0,001049	0,000151	0,00105	0,00015
40,37	0,0014	0	0,001177	0,000223	0,00118	0,00022
44,17	0,0016	0	0,001288	0,000312	0,00129	0,00031
47,29	0,0018	0	0,001379	0,000421	0,00138	0,00042
49,63	0,0020	0	0,001447	0,000553	0,00145	0,00055
51,27	0,0025	0	0,001495	0,001005	0,00150	0,00101
51,47	0,0024	0,00061	0,001501	0,000921	0,00150	0,00092
44,78	0,0030	0,13054	0,001305	0,001695	0,00150	0,00150
25,91	0,0035	0,49690	0,000755	0,002745	0,00150	0,00200

11.3 Appendix C - Numerical values for hand calculations

Table C.1: Steel notations

Part	Notation	Dimensions [m]
Width upper flange	$w_{up.f}$	0,25
Thickness upper flange	$t_{up.f}$	0,03
Height web	h_{web}	0,25
Thickness web	t_{web}	0,012
Width bottom flange	$w_{b.f}$	0,25
Thickness bottom flange	$t_{b.f}$	0,03

Table C.2: Concrete notations

Part	Notations	Dimensions [m]
Width concrete deck	w_c	1
Thickness concrete deck	t_c	0,17

Table C.3: Material properties steel

Property	Notations	Web [MPa]	Flange [MPa]
Yield stress	f_y	447	407
Ultimate stress	f_u	579	541
Modulus of elasticity	E	210 000	

Table C.4: Material properties concrete

Property	Notations	G1 [MPa]	G2 [MPa]
Compressive strength	f_{ccm}	54,8	51,5
Tensile strength	f_{ctm}	4,4	4,3
Modulus of elasticity	E	34300	33600

Check classification of cross section class

Calculated according to SS - EN 1993 - 1 - 1 (2005)

Control flanges

$$\varepsilon = \sqrt{235/f_y} = 0{,}76$$

C_{flange}=0,11 m

$$\frac{c}{t_f \varepsilon} = 4{,}85 < 9 => CS1$$

Control web

$$\varepsilon = \sqrt{235/f_y} = 0{,}73$$

C_{web}=0,23

$$\frac{c}{t_w \varepsilon} = 26 < 72 => CS1$$

Calculation of moment of inertia for non-composite girder

The moment of inertia for the cross section is calculated according to the parallel axis theorem (Isaksson & Mårtensson, 2019):

$$I_y = I_{yi} + A_i e_i^2$$

Moment of inertia for the steel beam:

$$I_y = \frac{t_{web} \cdot h_{web}^3}{12} + 2\left(W_f \cdot \frac{t_f^3}{12} + W_f \cdot t_f \cdot e^2\right) = 0{,}00031\ m^4$$

Distance between centre of gravity for the flanges to the centre of gravity for the whole cross section:

$$e = 0{,}14\ m$$

Calculation of moment of inertia for the concrete deck:

$$I_y = \frac{wh^3}{12} = 0{,}00041\ m^4$$

To be able to sum the moments of inertia for the steel and concrete parts, the ratio between the modulus of elasticity for the materials is used (Collin et al., 2012). It is calculated as:

$$r = \frac{E_{concrete}}{E_{steel}}$$

Total moment of inertia:
$I_{y,tot} = I_{steel} + r \cdot I_{concrete}$

Table C.5: *Moment of inertia non composite*

Girder	Reduction factor [-]	Moment of inertia [m^4]
$I_{y,tot,G1}$	0,16	0,00038
$I_{y,tot,G2}$	0,16	0,00038

Calculation of combined moment of inertia for concrete deck and steel beam with full composite action.

The moment of inertia for the cross section is calculated according to the parallel axis theorem (Isaksson & Mårtensson, 2019):

$$I_y = I_{yi} + A_i e_i^2$$

The variable e is the distance from the centre of gravity of the entire cross-section to the centre of gravity for each part. The total centre of gravity is calculated with:

$$e_{mc} = \frac{\sum A_i e_{i,i}}{A_i}$$

Table C.6: *Centre of gravity*

Girder	Centre of gravity [m]
$e_{mc,G1}$	0,30
$e_{mc,G2}$	0,28

The area and the moment of inertia for the concrete deck is reduced in the same way as previous calculation. The reduction factor is calculated as:

$$r_{Gi} = \frac{E_{concrete}}{E_{steel}}$$

Table C.7 and C.8 show the numerical values for the calculation of the moment of inertia. The reduction factor is used for the area and the moment of inertia for the concrete parts.

Table C.7: Calculation of the moment of inertia for Girder 1

Part	I_{yi} [m^4]	e [m]	A [m^2]	I_y [m^4]	$I_{steel}/I_{concrete}$ [m^4]
Flange	5,6E-07	0,29	0,0075	0,00061	0,00069
Web	1,6E-05	0,15	0,0030	7,9E-05	
Flange	5,6E-07	0,0056	0,0075	8E-07	
Concrete deck	6,7E-05	-0,094	0,028	0,00031	0,00031

Table C.8: Calculation of the moment of inertia for Girder 2

Part	I_{yi} [m^4]	e [m]	A [m^2]	I_y [m^4]	$I_{steel}/I_{concrete}$ [m^4]
Flange	5,6E-07	0,27	0,008	0,0005	0,00060
Web	1,6E-05	0,13	0,003	6E-05	
Flange	5,6E-07	-0,014	0,008	2E-06	
Concrete deck	6,6E-05	-0,114	0,027	0,0004	0,00042

Total moment of inertia:

$$I_{y,tot} = I_{steel} + I_{concrete}$$

Table C.9: Moment of inertia full composite

Girder	Moment of inertia [m^4]
$I_{y,tot,G1}$	0,001007
$I_{y,tot,G2}$	0,001015

Stresses due to bending moment

The stress over the cross section can be calculated from equations in Isaksson & Mårtensson (2019). Stress from bending moment:

$$\sigma = \frac{M \cdot e}{I}$$

For a simply supported beam, the maximum bending moment for point load of 350 kN is calculated with:

$$M_{max} = \frac{F \cdot L}{4} = 578\ kN$$

For a non-composite beam, the load is distributed between the concrete deck and the steel beam. To estimate the distribution of the load between the two parts, the ratio between the two different modulus of elasticity is used.

Table C.10: force acting on each part

Part	G1	G2
Steel	0,837 · F	0,840 · F
Concrete	0,163 · F	0,160 · F

Table C.11: Hand calculated stresses for non-composite action

Notation	G1 [MPa]	G2 [MPa]
$\sigma_{t.c.d}$	20	19
$\sigma_{t.u.f}$	241	242
$\sigma_{b.l.d}$	241	242

Table C.12: Hand calculated stresses for full composite action

Notation	G1 [MPa]	G2 [MPa]
$\sigma_{t.c.d}$	103	113
$\sigma_{t.u.f}$	5	16
$\sigma_{b.l.d}$	172	160

Displacement

The maximum displacement for a simply supported beam with simple beam theory is calculated as (Isaksson & Mårtensson, 2019):

$$u_{max} = \frac{FL^3}{48EI}$$

To make the displacement better replicate the laboratory tests, shear deformation is added for the web. When calculating the shear deformation, the flanges are neglected, and the force is assumed to only affect the web. The force acting on the steel is obtained from Table C.10 above.

The shear deformation is calculated as:

$$u_{s.d} = \frac{\frac{F}{2} \cdot \frac{L}{2}}{G \cdot A_w} = 2 \text{ mm}$$

The total deformation is calculated as:

$$u_{max} + u_{s.d} = u_{tot}$$

Table C.13: Displacement for a non-composite girder

Girder	F [kN]	L [m]	E [MPa]	I [m^4]	U_{tot} [mm]
G1_Steel	293	6,6	210 000	0,000311	29
G1_Concrete	57	6,6	34 300	0,00041	24
G2_Steel	294	6,6	210 000	0,000311	29
G2_Concrete	56	6,6	33 600	0,00041	24

Table C.14: Displacement for a full composite girder

Girder	F [kN]	L [m]	E [MPa]	I [m^4]	U_{tot} [mm]
G1	350	6,6	210 000	0,001007	10
G2	350	6,6	210 000	0,001015	10

11.4 Appendix D – Other descriptive pictures

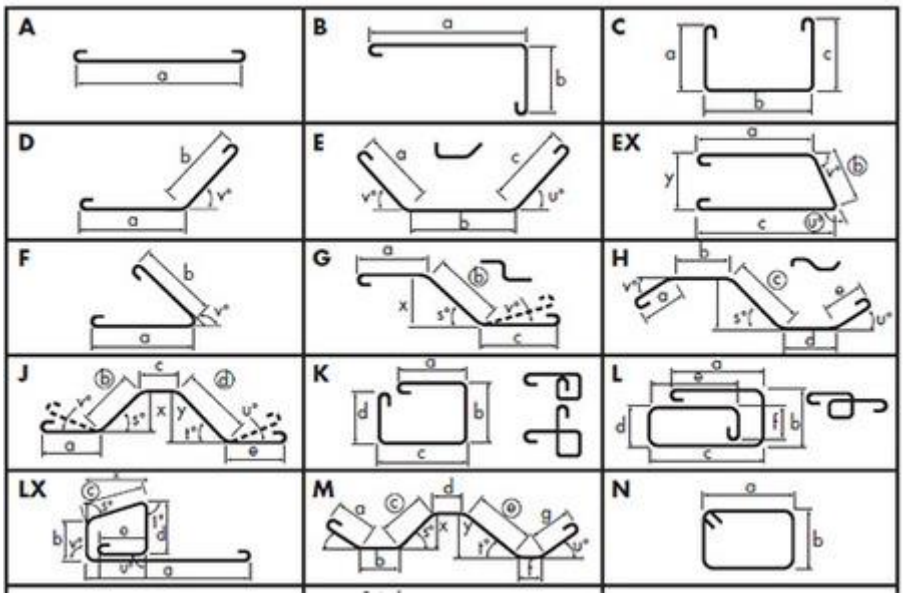

Figure D.1: Reinforcement bar types